

Article (refereed) - postprint

Wynn, P.M.; Ambler, S.; Grefe, I.; Soto, D.X.; Surridge, B.W.J.; Gabitov, R.I.; Barker, P.A.; Anwar, J.; Quin, A.; Pereira, M.G.; Grant, H.K.. 2021. **Contemporary systematics of vadose zone nitrate capture by speleothem carbonate.**

© 2020 Elsevier B.V.

This manuscript version is made available under the CC BY-NC-ND 4.0 license
<https://creativecommons.org/licenses/by-nc-nd/4.0/>



This version is available at <http://nora.nerc.ac.uk/id/eprint/529994>

Copyright and other rights for material on this site are retained by the rights owners. Users should read the terms and conditions of use of this material at <https://nora.nerc.ac.uk/policies.html#access>.

This is an unedited manuscript accepted for publication, incorporating any revisions agreed during the peer review process. There may be differences between this and the publisher's version. You are advised to consult the publisher's version if you wish to cite from this article.

**The definitive version was published in *Chemical Geology*, 157, 120172.
<https://doi.org/10.1016/j.chemgeo.2021.120172>**

The definitive version is available at <https://www.elsevier.com/>

Contact UKCEH NORA team at
noraceh@ceh.ac.uk

1 **Contemporary systematics of vadose zone nitrate capture by speleothem carbonate**

2
3 Wynn P.M^{a*}, Ambler, S^a, Grefe I^a, Soto D.X^b, Surridge, B.W.J^a, Gabitov, R.I^c, Barker, P.A^a, Anwar, J^a, Quin, A^a,
4 Pereira, M.G^b and Grant H.K^b

5
6 *^aLancaster Environment Centre, Lancaster University, Lancaster,*
7 *LA1 4YQ, UK.*

8 *^b UK Centre for Ecology and Hydrology, Lancaster, LA1 4AP, UK*

9 *^cDepartment of Geosciences, Mississippi State University, Mississippi State, MS 39762, United States.*

10
11
12
13
14
15
16
17
18
19
20 * Corresponding author. E-mail address: p.wynn@lancaster.ac.uk

25 **Abstract**

26 The movement of nitrate through the vadose zone has major implications for environmental and human health.
27 This issue is particularly prevalent in karst terrain where agricultural activity, thin soils and dual permeability
28 compound the problem of high nitrate loading to the overlying ecosystem. However, a paucity of records which
29 document vadose zone nitrate concentrations prior to the 21st century render legacy nitrate dynamics, source
30 attribution and baseline conditions to be poorly parameterised. Speleothems growing within karst cave settings
31 may provide an opportunity to obtain records of vadose zone nitrate contamination which extend throughout the
32 anthropogenic era. Here, we use dual isotope analysis of $\delta^{15}\text{NNO}_3$ and $\delta^{18}\text{ONO}_3$ in a contemporary study at Cueva-
33 cubío del Llanío, N. Spain, designed to examine the transformation of nitrate between surface to cave
34 environment, taking account of biogeochemical transformation, karst hydrology and partitioning as controls on
35 the delivery of nitrate to the speleothem record. Concentrations of nitrate within speleothem calcite are low
36 (measured range of 0.05mM to 0.37mM) due to partitioning (DNO_3) across the dripwater-calcite interface. Values
37 of $\delta^{15}\text{NNO}_3$ extracted from cave waters in Cueva-cubío del Llanío (range +2.0 to +7.0‰) are shown to be excellent
38 indicators of nitrate source and demonstrate no fractionation during incorporation into speleothem carbonate
39 (range of $\delta^{15}\text{NNO}_3$ in speleothem carbonate +1.6‰ to +6.4‰). Values of $\delta^{18}\text{ONO}_3$ contained within cave waters
40 (range -2.5‰ to +6.0‰) and speleothem carbonate (range +12.3‰ to +32.3‰) reflect a mixed signal of source,
41 biogeochemical processing and hydrological pathway, providing critical insight into the behaviour of the karst
42 aquifer. Contemporary systematics at Cueva-cubío del Llanío therefore confirm speleothem carbonate contains
43 an excellent record of vadose zone nitrate. Analysis of nitrate contained within speleothem carbonate from other
44 regions confirms the ubiquitous nature of partitioning across the water-carbonate interface and the use of
45 speleothem nitrate isotopes for recording surface ecosystem processes and vadose zone behaviour. Application
46 of these principles to dated speleothem records should provide critical timeseries of nitrate loading, enabling
47 understanding and remediation against the presence of vadose zone legacy nitrate.

48

49 **1. Introduction**

50 Loading of reactive nitrogen to the global biogeochemical cycle is impacted heavily by anthropogenic activity.
51 Industrial pollution releases nitrogen compounds into the atmosphere, and intensification of agricultural practices
52 exacerbates the input of reactive nitrogen to the biosphere through the application of organic materials and
53 inorganic fertilisers. The resultant fluxes of reactive nitrogen can adversely affect freshwater ecosystems through
54 eutrophication and acidification, as well as impact human health through nitrate contamination of groundwater
55 used for drinking water supplies (eg. Vitousek, 199; Galloway et al., 2008; Matiatos et al., 2021). However, the
56 loss of reactive nitrogen to the vadose zone, where leaching from surface to groundwater and slow transit times
57 leads to the longterm storage of nitrate is poorly quantified (Ascott et al., 2017). Retention of nitrate in the
58 vadose zone has created a 'nitrate time bomb', whereby the impact of peak N application has been delayed to
59 create a problem for future generations (Wang et al., 2013). Despite recent controls on anthropogenic nitrogen
60 loading in some countries, many environmental systems will continue to suffer from 'legacy nitrate' on a
61 timescale which depends upon the storage and release dynamics of vadose systems. This is particularly the case
62 for karstic bedrock which forms a significant proportion of the global vadose zone, with over a quarter of the
63 World's population relying on water sourced from karst regions (Ford and Williams, 2013). Karst systems present
64 a unique hydraulic configuration, comprising dual permeability characteristics of rapid fracture and slow matrix
65 flow. Thin soils and fracture pathways convey surface pollution rapidly into the vadose system, making them
66 acutely vulnerable to contamination, whilst the remaining pollutant load can become entrapped within the matrix
67 porosity of the carbonate bedrock, forming a significant store of legacy nitrate within the vadose zone. However,
68 whilst empirical observations of karst vadose zone nitrate dynamics are reasonably well studied over event based
69 to decadal time scales (eg. Jiménez-Sánchez et al., 2008; Husic et al., 2019a,b and compilation of references
70 therein; Yue et al., 2018; Yue et al., 2019; Yang et al., 2020), observations prior to 21st century monitoring are
71 rare. This leaves a lack of knowledge regarding baseline pre-industrial vadose zone nitrate concentrations, no
72 information on changing nitrate sources prior to the 21st century and no empirically determined rates of nitrate

73 transfer through the dual permeability karst vadose zone system. Where nitrogen biogeochemical cycling can be
74 traced through the soil-karst system using stable isotopes, and the incorporation of nitrogen species into calcium
75 carbonate can be parametrised, speleothems (cave stalagmites and stalactites) growing in karst regions could be
76 used to overcome this lack of knowledge, providing a natural, time-resolved archive of vadose zone nitrate
77 dynamics. Stalagmites growing in cave environments incorporate trace elements and nutrients delivered from the
78 overlying vadose zone of karst storage, via drip waters. The drip water record will therefore be incorporated into
79 speleothem calcite reflecting surface loading and the lag time associated with vadose zone storage. The nitrogen
80 content of speleothem calcite which has grown consistently throughout the past ~200 years could ultimately
81 enable contextualisation of surface nitrogen loading, recording time-bomb type waves of nitrate passing through
82 the vadose zone prior to entering the deeper groundwater system. However, the linkage between groundwater
83 legacy nitrate and the speleothem record initially needs to take into account biogeochemical modification of
84 surface inputs, karst transfer and partitioning into contemporary carbonate deposits. Here, we use stable
85 isotopes to trace the movement of nitrate between surface pasture ecosystem to cave drip waters and associated
86 contemporary speleothem deposits. We specifically address the ability of contemporary speleothem carbonate to
87 accurately represent the chemical and isotopic signature of dripwater nitrate, thereby unlocking the potential for
88 stalagmites which have grown throughout the 19th to 20th centuries to provide a time-resolved record of vadose
89 zone nitrate dynamics.

90

91 **2. Karst nitrogen biogeochemical cycling and transfer into carbonate**

92 2.1. Nitrogen biogeochemical pathways in karst ecosystems

93

94 Biogeochemical modification of surface inputs serve to control the entry of nitrate into the vadose zone,
95 potentially also modifying isotopic signatures away from source values. Biogeochemical cycling of nitrogen
96 typically consists of five key processes 1. Nitrogen fixation (bacterial fixing of atmospheric N₂ into the organic
97 phase), 2. Mineralisation and nitrification (representing the overall conversion of organic N to ammonia and then
98 to nitrate within the soil/root zone), 3. Assimilation (uptake of soil ammonia and nitrate into the organic phase),
99 4. Volatilisation (vaporisation of ammonia compounds from the soil surface in the aftermath of application) and 5.
100 Denitrification (the conversion of oxidized nitrogen compounds to N₂ gas under conditions of low oxygen status).

101 Nitrogen fixation causes only limited nitrogen isotope fractionation (-2 to +2‰) (Casciotti, 2009 and references
102 therein), and denitrification would not be expected to play a large role in the karst biogeochemical nitrogen cycle
103 due to limited potential for the development of anoxia within the karst vadose zone and overlying soils. The three
104 main fractionating processes of concern to karst environments are therefore volatilisation, assimilation and
105 nitrification. The extent to which these biogeochemical processes modify source signatures away from
106 recognisable end-member isotopic values is dependent upon site-specific antecedent conditions controlling the
107 degree of fractionation inherent in each.

108 Volatilisation is known to cause extensive loss of ammonia to the atmosphere (Cameron et al., 2013) and
109 equilibrium isotopic fractionation during volatilisation is documented as approximately +30‰, thereby enhancing
110 the residual soil ammonium pool in ¹⁵N (Heaton, 1986). However, in karst ecosystems dominated by pasture
111 grazing and which are replete in nitrogen, there is reportedly limited potential for this enriched signature to be
112 translated directly into nitrate leachates due to overprinting of the residual ammonium isotopic signature by soil
113 mineralisation and nitrification (Wells et al., 2015).

114 Fractionation during assimilation causes ¹⁵N depletion in plant-based tissues relative to the substrate isotopic
115 composition. Measured fractionation varies between 0‰ to +12.6‰ for net ammonia assimilation into plants
116 (Evans, 2001 and references therein) and 0‰ to +18‰ for net nitrate assimilation into plants under open system
117 conditions (Liu et al., 2014 and references therein; Evans, 2001 and references therein), thus generating a residual
118 soil pool enriched in ¹⁵N. However, the impact of assimilation and associated kinetic fractionation upon the soil N
119 pool is largely dependent upon whether the soil system is representative of an open or closed system. In an open
120 system where soil N supply continuously exceeds demand, fractionation will produce an offset between plant and

121 soil, although the soil isotopic composition will not change over time. Under closed or semi-closed system
122 conditions where soil N supply cannot always satisfy demand, substrate concentration will decline through time.
123 Both soil substrate and plant N will gradually become enriched in ^{15}N and assimilated plant N will converge on the
124 initial soil substrate isotopic composition. Karst ecosystems supporting an agricultural land use are replete in
125 nitrogen and likely follow the principles of an open system, such that assimilative activity has little effect upon soil
126 nitrogen isotopic status. However, karst ecosystems supporting natural vegetation are more likely to be nitrogen
127 limited, thus causing temporal variation in the soil substrate isotopic composition. The open/closed nature of a
128 karst system will also be dependent upon the seasonality of plant demand for nitrogen.

129 The overall conversion of organic-N to nitrate comprises mineralisation (the conversion of organic N to ammonia)
130 and nitrification (the oxidation of ammonia to nitrate). Mineralisation rarely causes fractionation (eg. Heaton et
131 al., 1986; Högberg, 1997). However, the nitrification of ammonium to nitrite causes a kinetic fractionation to $\delta^{15}\text{N}$
132 which ranges between +24.6‰ to +38.2‰ based on terrestrial strains of ammonia oxidizing bacteria
133 (*Nitrosospira tenuis*, *Nitrosomonas eutropha*, and *Nitrosomonas europaea*) (Casciotti et al., 2003 and references
134 therein). The conversion of nitrite to nitrate is associated with an inverse isotopic fractionation of -12.8 +/- 1.5‰
135 (*Nitrococcus mobilis*, Casciotti, 2009). The overall fractionation for the entire nitrification pathway is dependent
136 upon environmental conditions and the relative dominance of substrate pool size. Where the system is nitrogen
137 limited, the rate-determining step is represented through the mineralisation of organic-N to ammonia. As
138 mineralisation supports limited fractionation, the $\delta^{15}\text{N}$ of product nitrate will closely resemble the isotopic
139 composition of the total organic nitrogen (Heaton et al., 1986). However, where the substrate ammonium is in
140 abundant supply, initial oxidation products may be expected to be isotopically depleted in ^{15}N . As the ammonium
141 substrate pool becomes depleted in abundance, isotopic fractionation should approach unity, such that nitrate
142 oxidation products are of similar isotopic value to initial ammonium signatures. In karst systems supporting
143 agricultural activity, nitrogen availability should be replete and product soil water should be isotopically depleted
144 compared to source. For those karst systems which are not impacted by agriculture, soil water nitrate will be
145 representative of N source. During nitrification, the stoichiometric incorporation of oxygen into the nitrate
146 molecule comprises a maximum 1:2 ratio of oxygen sourced from O_2 and H_2O , although discrepancies to this
147 theoretical rule may be expected in natural systems (eg. Mayer et al., 2001 ; Venkiteswaran et al., 2019 ;
148 Romanelli et al., 2020). The oxidation of ammonia to nitrite utilises oxygen from O_2 and H_2O in equal proportions,
149 but also encompasses an isotopic fractionation to $\delta^{18}\text{O}$ during the incorporation of each which can be collectively
150 parameterised as +19.3+/-2.9‰ (bacterial strain *Nitrosomonas europaea*) or +30.3 +/-1.0‰ (bacterial strain
151 *Nitrosospira briensis*, Casciotti et al., 2010). The exchange of oxygen between nitrite and water also has the effect
152 of causing an equilibrium isotopic fractionation of approximately +14‰ (Casciotti et al., 2007). The oxidation of
153 nitrite to nitrate incorporates one oxygen atom sourced from water into the nitrite molecule (isotopic
154 fractionation parameterised as +12.8‰ to +18.2‰, Buchwald and Casciotti, 2010). Fractionation also occurs at
155 the point of nitrite oxidation, and during oxygen atom exchange with water although these two sources are noted
156 to be minimal under oxidizing conditions where nitrite availability is low (Buchwald and Casciotti, 2010). Within
157 karst systems where nitrate is sourced as a product of nitrification, values of $\delta^{18}\text{ONO}_3$ will therefore lie between a
158 defined upper and lower threshold dependent upon the water-oxygen isotopic composition and the range of
159 fractionation factors employed.

160

161 The overall impact of biogeochemical cycling and fractionation in karst systems thus depends upon whether the
162 system is considered open or closed, and replete or limited in nitrogen. Where karst systems are nitrogen limited
163 and predominantly closed to excessive new inputs, volatilisation will be limited, assimilation will progress towards
164 completion and the nitrification pathway will be controlled by mineralisation, causing minimal fractionation to
165 $\delta^{15}\text{NNO}_3$. Nitrate isotopic signatures entering into the vadose zone will thus reflect those of surface inputs, with an
166 expressed seasonality in $\delta^{18}\text{ONO}_3$ dependent upon the relative significance of nitrifying activity. However, where
167 karst soils support agricultural activities, the system must be considered open and replete in nitrogen.
168 Volatilisation will be extensive, although any associated isotopic fractionation will be largely overprinted by the
169 nitrification pathway. Assimilation will have limited effect on the isotopic composition of the soil substrate N pool.
170 Under this scenario, nitrate isotope values present in cave drip waters will likely be depleted in ^{15}N compared to
171 source signatures. Both $\delta^{15}\text{NNO}_3$ and $\delta^{18}\text{ONO}_3$ may express pronounced seasonality dependent upon the extent of
172 nitrification occurring within the soil zone.

173 2.2 Transfer of nitrate through karst and into speleothem carbonate

174 The complex drainage structure of karst systems serves to modify isotopic signatures of nitrogen biogeochemical
175 cycling away from those identified at the base of the soil zone. The dual permeability of karst bedrock comprises a
176 rapid fracture flow and a slow matrix flow system. Whereas the fracture system is ephemeral, matrix systems fill
177 during times of water excess to deliver a steady water flux over a prolonged period of time. Where rapid fracture
178 flow is the dominant hydrological pathway, water demonstrates little storage or mixing within the karst. Water
179 can be of meteoric origin or from the soil zone, with associated nutrient signatures being routed through the karst
180 with such rapidity as to obviate any isotopic differences due to vadose zone processes (eg. Wynn et al., 2013).
181 However, within the slow matrix flow system, storage and mixing can occur across multiple timescales to create a
182 nitrogen signal which reflects a homogenisation of sources and biogeochemical processes, otherwise known as
183 legacy nitrate. Soil waters charged with carbonic acid will also come into prolonged contact with carbonate
184 bedrocks, and dissolution of the host bedrock will release constituent trace ions into solution. This bedrock end
185 member may contribute sufficient N to control the composition of the dripwater solution if nitrogen
186 concentrations are high and/or support an isotopic value which is distinctly different to the aqueous solution. An
187 upper estimate of nitrogen contribution from bedrock dissolution can be calculated as follows $\% \text{bedrock NO}_3 =$
188 $[1/(\text{bedrock Ca+Mg:NO}_3/\text{dripwater Ca+Mg})/\text{dripwater NO}_3] \times 100$. This equation is based on Wynn et al., 2008, assuming only
189 limited contributions of calcium and magnesium from extraneous sources such as rainfall, plant necromass and
190 organic fertilisers, alongside limited impact of prior calcite precipitation upon drip water ratios to nitrate). Where
191 a component of slow matrix flow contributes to the hydrological regime, the biogeochemical signature conveyed
192 in cave drip waters is therefore not a direct reflection of source (atmospheric deposition or soil zone
193 biogeochemistry), but also represents hydrological pathway, time-integrated storage dynamics, and additional
194 inputs from bedrock dissolution.

195 When cave drip waters actively deposit calcium carbonate onto speleothem growth surfaces, the nitrate ion can
196 become incorporated into the calcite (Kontrec et al., 2004). The incorporation mechanism, however, remains
197 unresolved. Partition co-efficients of the form $\text{DNO}_3 = (\text{NO}_3/\text{CO}_{3\text{solid}})/(\text{NO}_3/\text{CO}_{3\text{solution}})$ have also yet to be
198 established (cf. Wynn et al., 2018) and associated controls on incorporation identified through controlled calcite
199 growth experiments. Any degree of isotopic fractionation across the aqueous-solid interface is also in need of
200 parameterisation. The bulk nitrate signature conveyed within cave drip waters comprising source signature, soil
201 biogeochemical processing, bedrock dissolution, karst attenuation and mixing, will thus be incorporated into
202 speleothem calcite at a temporal resolution dependent upon growth rate. Where isotopic signatures can be
203 deconvolved according to the above framework of biogeochemical cycling and phase boundary partitioning,
204 information on changes in nitrogen source can be obtained. Time-resolved changes in speleothem concentration
205 dynamics can be used to determine vadose zone storage and thus legacy effects within karst landscapes, as well
206 as pre-anthropogenic baseline status. Speleothems could thus become one of the most significant archives of
207 legacy nitrate dynamics, providing a record of sufficient longevity for the improvement and testing of existing
208 empirical groundwater models.

209

210 3. Methodology

211 3.1 Cave site description and sample collection regime

212 Cueva-cubío del Llanío is a shallow cave system located within the Cantabrian Cordillera of N. Spain
213 (43°21'29.9"N, 003°35'53.8"W, 165 m a.s.l.). It is located within the Riaño valley, 21 km south east of Santander,
214 forming part of a connected network of caves which link to those of the neighbouring Matienzo depression (eg.
215 Smith et al., 2015, 2016a,b). The cave is developed in Lower Cretaceous (Aptian-Albian) carbonate of shallow
216 water platform origin (Dewitt et al., 2014; Aranburu et al., 2015), with host bedrock comprising a mixed calcite-
217 dolomite composition (70% dolomite content calculated following Fairchild and Treble, 2009), interbedded with
218 sandstones and marl (Gutiérrez, 2010). The soil is organic rich and with loamy texture, often in excess of 50 cm
219 depth, supporting a clover-rich pasture of variable grazing intensity. Cave drip waters were sampled on a seasonal

220 basis from two chambers which supported contrasting surface vegetation characteristics (Figure 1). High Hopes
221 chamber was located at a depth of approx. 14 m beneath managed pastureland formerly fertilised with manure
222 (manure application ceased in 2017), whereas Whoopee Hall was located at a shallower depth of approx. 5 m
223 beneath steeply sloping pasture with low intensity grazing and minimal manure application.

224 Drip sites in High Hopes chamber support a range of hydrological characteristics. High Hopes drips 1-6 are
225 delivered via soda straw stalactites and feed actively depositing speleothems. Each drip is predominantly matrix
226 fed, albeit with flow recession during the summer months reflecting the seasonality of rainfall dynamics within
227 the region (eg. Smith et al., 2016b). Drip water discharges range between 64 ml to 598 ml per day, with greatest
228 sensitivity to rainfall events being observed during the winter season (see drip logger record for High Hopes 2 and
229 3 in Figure S1). Fast drips 1 and 2 are located approx. 5 meters away within the same chamber, albeit represent a
230 more ephemeral flow of water entering into the cave and are likely to be at least partially fracture fed. The drip
231 site in Whoopee Hall delivers dripwater from a soda straw stalactite onto an actively growing stalagmite.
232 Dripwater discharge is up to 711 ml per day. A persistent winter discharge, albeit with flow cessation during the
233 summer months at this site is suggestive of a predominantly matrix fed hydrology, albeit from a reservoir of
234 sufficiently limited volume to prevent year-round flow characteristics (see drip logger record for Whoopee Hall in
235 Figure S1). Pool waters within both chambers were fed by the ephemeral, fracture flow drip sites.

236 Each drip site was sampled over a time interval commensurate with discharge characteristics. For those sites
237 where water flow was sufficient, samples were collected instantaneously during a typical 4-hour period within the
238 cave. Drip site High Hopes 1 supported a sufficiently slow drip rate to enable sample collection only on seasonally
239 scheduled visits to the cave. All other drip sites had water samples collected over a 24-hour period. Pool waters
240 within the cave were ephemeral and thus sampled whenever possible during scheduled cave visits. After drip and
241 pool water collection, samples were tested for pH, EC (electrical conductivity) and temperature. One aliquot of
242 each sample (approx. 30 ml) was filtered through a 0.2 micron membrane (polyethersulfone) filter and stored
243 frozen (-20°C) within a Nalgene LDPE bottle. Any remaining water up to a maximum of 60 ml was stored
244 unfiltered and refrigerated prior to further analysis. Rainfall dynamics were monitored in the neighbouring village
245 of Matienzo using a Pluvimate drip logger (Driptych.com) to record both rainfall intensity and volume (see record
246 provided in Figure S1). Rainfall was also collected for nitrate isotopic analysis as monthly bulk collections on an
247 ad-hoc basis. Soil and vegetation samples were collected from above the cave to monitor nitrogen content and
248 isotopic composition. Soil samples were collected as composite cores up to 10 cm in depth, and vegetation
249 samples were collected from the same locations. Sediment samples were collected from within the cave system
250 to represent an integrated sample of inwashed material and cave internal breakdown products.

251 Modern speleothem calcite was grown on either glass plates (up-turned watch-glasses pre-cleaned using an acid
252 wash, no etching used to encourage calcite nucleation) or stalagmate logger surfaces placed beneath each of the
253 drip sites defined above, and left to deposit for approximately 6 months between collections. Upon removal from
254 the cave, the calcite deposit was removed using a scalpel. Samples were homogenised and stored prior to analysis
255 for nitrate concentration and isotopic composition. Archived speleothem samples were used to expand the
256 speleothem nitrate data set to cave sites with differing vegetation characteristics and nitrogen inputs. These sites
257 comprised stalagmites collected from Rukiesa Cave, Ethiopia (Asrat et al., 2007, 2008; Baker et al., 2007), Browns
258 Folly Mine, Somerset, UK (Baker et al., 1998, 1999a; Baldini et al., 2001, 2005; Fairchild et al., 2006), and Ease Gill
259 Cavern, Cumbria. Calcite grown on glass plates in Cueva de las Perlas, Matienzo, N. Spain (Deeprise, 2018) and
260 Pooles Cavern, Buxton, UK (Baker et al., 1999b; Baker and Genty, 1999; Hartland et al., 2010, 2011, 2012; Newton
261 et al., 2015) were also utilised for nitrate extraction. Carbonate powders which represented the most recent
262 speleothem growth prior to collection were extracted from all samples other than Ease Gill Cavern. At this latter
263 site, the fossil nature of the speleothem provided an opportunity to obtain a pre-anthropogenic sample.

264

265 **3.2 Laboratory methodology**

266 Nitrate concentrations in cave dripwater, pools and rainfall, were analysed from the filtered water aliquot using
267 automated colourimetry (SEAL AQ2 analyser), based on the cadmium reduction of nitrate to nitrite with an
268 analytical range of 0.06 to 5 mg l⁻¹ NO₃-N and a limit of detection (LOD) of 0.01 mg l⁻¹ NO₃-N. Concentrations were
269 not corrected for the presence of nitrite, due to it being below the range of the AQ2 analyser within a
270 representative subset of samples (analytical range of 0.01 to 0.1 mg l⁻¹ NO₂-N). Concentrations of ammonia were
271 determined on the same sample aliquots by SEAL AQ2 analyser, based on indophenol blue colourimetry and with
272 an analytical range between 0.02 to 2 mg l⁻¹ NH₄-N. For both techniques analytical precision based on the repeat
273 analysis of reference standard material (0.25 mg l⁻¹ and 1 mg l⁻¹ N for both nitrate and ammonia analysis) is
274 reported to within 5% of expected values. The total carbonate composition of aqueous samples was determined
275 using titration with phenolphthalein and Bromocresol indicators. The cation composition of cave waters (Ca, Mg)
276 was analysed by Inductively Coupled Plasma Optical Emission Spectroscopy (ICP-OES), at Lancaster University, UK,
277 using a Thermo Scientific iCAP 6000. Each sample was acidified using ultrapure nitric acid to achieve a final
278 concentration of 0.1M, matrix matched to standard solutions. Repeat analysis of reference standard material
279 (concentration of 1 mg l⁻¹ for all species analysed) is reported to within 5% of expected values.

280 Nitrate isotope analysis was undertaken on drip water samples using the microbial denitrifier technique (Sigman
281 et al., 2001; Casciotti et al., 2002) at the Lancaster Environment Centre, Lancaster University, UK. This technique
282 used cultures of *Pseudomonas chlororaphis*, a denitrifying bacterium lacking nitrous oxide reductase, to convert
283 20 nmol of sample nitrate to nitrous oxide. Speleothem and bedrock carbonates were also analysed for nitrate
284 isotopic content using the microbial denitrifier technique. Sufficient speleothem powder (typically 100 mg) was
285 dissolved stoichiometrically in ultrapure 1M hydrochloric acid to a neutral pH. The reaction was undertaken at
286 room temperature to prevent any oxygen isotopic exchange between nitrate and water under low pH (Kaneko
287 and Poulson, 2013). After carbonate dissolution, the digestate was diluted to 5 ml with de-ionised water and the
288 whole sample injected into 20 mL headspace vials containing the bacterial cell suspension. For both drip waters
289 and carbonates, the headspace nitrous oxide was subsequently injected into an Isoprime Trace gas
290 preconcentrator inlet and autosampler, coupled to an Isoprime Isotope ratio Mass Spectrometer (IRMS) at the
291 NERC National Environmental Isotope Facility (NEIF) at CEH Lancaster, UK. International reference materials
292 (USGS-34, USGS-35 and IAEA-NO-3) were used for calibration, assuming $\delta^{15}\text{N}$ values of -1.8‰ and +4.7‰ for
293 USGS 34 and IAEA-NO-3, and $\delta^{18}\text{O}$ values of -27.9‰, +57.5‰ and +25.6‰ for USGS-34, USGS-35 and IAEA-NO-3
294 respectively. Within-run standard precision for both international and in-house standards was <0.2‰ and <0.5‰
295 (1SD) for $\delta^{15}\text{NNO}_3$ and $\delta^{18}\text{ONO}_3$ respectively. Triplicate analysis of selected samples in each run sequence (both
296 cave waters and speleothem digests) yielded sample analytical precision within the same range. Background
297 contamination (analysis of microbial culture without sample inoculation) averaged 0.7% (range 0.5% to 1.4%) of
298 the in-house standard peak area. To test for matrix effects during speleothem nitrate isotopic analysis, a
299 carbonate with low nitrate content was digested following the protocol above and spiked with the in-house
300 standard prior to analysis with the denitrifier method. $\delta^{15}\text{NNO}_3$ and $\delta^{18}\text{ONO}_3$ values were within error (1SD
301 precision) of values expected for the internal standard, showing no discernible matrix effects from the acid digest.
302 The nitrate concentration contained within each cave water, speleothem and bedrock carbonate analysis was
303 determined by peak area integration using IonVantage software.

304 Determination of total nitrogen content and isotopic composition within vegetation, sediment and soil samples
305 was undertaken at the Lancaster Environment Centre stable isotope laboratory, Lancaster University using an
306 Elementar varioMICRO elemental analyser interfaced to an Isoprime 100 continuous-flow isotope ratio mass-
307 spectrometer. Vegetation samples were dried at 50 °C for 24 hours, crushed and homogenised. Sediment and soil
308 samples were dried at 50 °C for 48 hours, sieved to remove any large rock fragments and subsequently crushed.
309 Combustion of samples within tin capsules at 950 °C yielded N₂ for analysis of $\delta^{15}\text{N}_{\text{total}}$. Within-run replication of
310 international and in-house standards was better than 0.3‰ (1SD) for $\delta^{15}\text{N}$. Concentrations of total nitrogen were
311 calculated using peak area integration in the varioMICRO software, calibrated to within-run determinations of
312 acetanilide.

313

314 3.3 Mixing models

315 A Bayesian isotope mixing model (MixSIAR operated in open-source R software, Stock and Semmens, 2013) was
316 used to determine the relative proportion of nitrate sources (e.g. Soto et al. 2019) in cave waters and
317 contemporary speleothem calcite. The end-member sources for dissolved nitrates used to drive the model
318 comprised (1) manure ($+13.0 \pm 4.3$ for $\delta^{15}\text{N}$ and -8.45 ± 2.20 for $\delta^{18}\text{O}$), (2) precipitation ($+1.00 \pm 1.64$ for $\delta^{15}\text{N}$ and
319 $+66.48 \pm 3.67$ for $\delta^{18}\text{O}$), and (3) NO_3 derived from the nitrification of rainfall NH_4^+ and re-mineralisation of fixed N_2
320 (-2.5 ± 2.50 for $\delta^{15}\text{N}$ and -8.45 ± 2.20 for $\delta^{18}\text{O}$). The nitrogen and oxygen isotopic composition of precipitation
321 nitrate was determined from samples collected in the study area. The $\delta^{15}\text{N}$ values for (1) and (3) were taken from
322 the literature (Kendall et al. 2007, Chalk et al. 2019) and $\delta^{18}\text{O}$ values were estimated based on the range of
323 expected values for theoretical nitrification in the system (calculated to range between -15.0‰ to -1.9‰).
324 Inorganic fertilizers are not used in the pastures above the cave, therefore this nitrate source was not considered.
325 We assumed that after conversion of inputs to nitrate, mixing below the soil zone occurred conservatively and
326 further fractionation through biogeochemical cycling was deemed negligible. As nitrate isotopic signatures
327 sourced from the re-mineralisation and nitrification of fixed N_2 cannot be isotopically distinguished from the
328 nitrification of rainfall ammonium, these two inputs were considered as a single source in the model. For each
329 type of material, a Bayesian mixing model was run with three chains of 300,000 iterations, a burn-in of 200,000
330 and a thinning of 100; including 'cave chamber' and 'water type' as fixed variables. All cave waters and
331 contemporary speleothem calcite samples fall inside the mixing polygon formed by the sources.

332

333 4. Results

334 Concentrations of nitrogen and $\delta^{15}\text{NNO}_3$ values for all measured aqueous (cave waters and rainfall), soil / sediment
335 and vegetation samples are compiled and presented within Table 1 (full underlying dataset available through the
336 data repository at <http://dx.doi.org/10.17635/lancaster/researchdata/xxx>). Rainfall forms the most dilute end
337 member component of the system (arithmetic average rainfall concentration = 0.01 mM $\text{NO}_3\text{-N}$). The soils above
338 the cave and sediments within the cave support concentrations of total nitrogen ranging between 35.7 to 461.9
339 mM (per kg) and vegetation growing immediately above High Hopes chamber contains the greatest total nitrogen
340 content of all measured components (range 1555.3 to 2599.0 mM, per kg) (Table 1). Cave water nitrate
341 concentrations plot intermediate to the rainfall and soil/sediment end-members (Figure 2). Ammonia-nitrogen is
342 present within rainfall at low concentrations (average 0.012 mM, range 0.006 mM to 0.021 mM). In cave waters
343 ammonia-nitrogen is present on just three separate sampling occasions, with inconsistent presence across drip
344 sites (average 0.006 mM, range 0.002 mM to 0.017 mM). On all other occasions, ammonia-nitrogen in drip and
345 pool waters is below detection.

346 Values of $\delta^{15}\text{NNO}_3$ show clear distinction between rainfall and soil/sediment sources, such that rainfall forms the
347 lightest isotopic end member (arithmetic average $+1.0\text{‰}$, range -1.3‰ to $+3.0\text{‰}$), compared to soils and
348 sediments (average $+5.2\text{‰}$, range $+2.3\text{‰}$ to $+8.0\text{‰}$). Cave drip and pool waters support $\delta^{15}\text{NNO}_3$ signatures that
349 are similar in composition to the soils/sediments (average $+5.5\text{‰}$, range $+2.0\text{‰}$ to $+7.0\text{‰}$) (Figure 2). There is an
350 isotopic shift in $\delta^{15}\text{NNO}_3$ between the two cave chambers with waters in High Hopes chamber appearing more
351 enriched in ^{15}N than those in Whoopee Hall (Figure 3). Whereas bedrock samples collected from within the cave
352 demonstrate similar isotopic composition to the drip and pool waters (bedrock average $\delta^{15}\text{NNO}_3 = +4.5\text{‰}$),
353 bedrock dissolution is calculated to comprise an upper estimated contribution of 0.24% of the dripwater NO_3
354 (calculated using ratios of calcium + magnesium to nitrate following methods in Wynn et al., 2008), confirming
355 minimal impact on drip water isotopic signature. The $\delta^{15}\text{N}$ composition of vegetation growing above the cave
356 ranges between -1.1‰ to $+2.3\text{‰}$ (Table 1). Whilst $\delta^{18}\text{ONO}_3$ values of rainfall range between $+62.3\text{‰}$ to $+71.9\text{‰}$, a
357 distinct shift in isotopic signature is apparent between rainfall and cave waters (Figure 3), with cave water $\delta^{18}\text{ONO}_3$
358 composition ranging between -2.5‰ to $+6.0\text{‰}$.

359 Nitrogen concentrations and isotopic compositions have also been measured from modern speleothem
360 carbonate grown within each cave chamber at Cueva-cubío del Llanío (Table 2). Concentrations of nitrate range

361 between 0.05 to 0.37 mM NO₃. The relative efficiency of nitrate partitioning between drip waters and speleothem
362 calcite (DNO₃^{x10⁻⁵}) is quantified as ranging between 0.06 to 0.42 across both cave chambers when substituting for
363 carbonate (Table 2). On average, δ¹⁵NNO₃ signatures in contemporary speleothem calcite (average +4.5‰, range
364 +1.6‰ to +6.4‰) are enriched compared to those in the input rainfall (average +1.0‰, range -1.3‰ to +3.0‰),
365 but show no difference in value compared to the source cave waters. The δ¹⁸ONO₃ composition of modern
366 carbonate lies between rainfall and cave water signatures (Figure 3). Analysis of nitrate concentration and
367 isotopic composition is also extended to speleothems sourced from cave sites in other regions (Figure 4). Nitrate
368 concentration shows a wide range in values from 0.02 to 0.86 mM NO₃, dependent on speleothem growth setting
369 (Table 3). Where coeval drip water and speleothem chemistry have been obtained, this extends the range of
370 DNO₃^{x10⁻⁵} up to the value of 1.43 (Table 2). The range in speleothem δ¹⁵NNO₃ is narrow (range +2.1 to +6.0‰),
371 reflecting the restricted range in δ¹⁵N composition from source materials (Table 3). However, the δ¹⁸ONO₃ isotopic
372 composition extends from +6.0‰ to +58.6‰, representative of end member materials and the extensive
373 fractionating effects endured through biogeochemical cycling.
374

375 5. Discussion

376 Interpreting groundwater nitrate dynamics from speleothem calcite requires understanding of source signatures,
377 biogeochemical cycling and hydrological routing through karst. Isotopic fractionation adjusts signatures from
378 source composition and partitioning of nitrate between water and calcite will offset speleothem concentration
379 profiles from true groundwater characteristics. Here, we use knowledge from the fields of nitrogen
380 biogeochemical cycling, groundwater hydrology and carbonate chemistry, to trace the evolution of nitrogen
381 inputs from source to speleothem. We use this to build an appreciation for the potential of age-constrained
382 speleothem records to provide an archive of groundwater nitrate dynamics.

383 5.1 The nitrate composition of cave dripwaters

384 The nitrogen biogeochemical cycle at Cueva-cubío del Llanío is known to comprise three main inputs: rainfall,
385 manure-derived nitrogen and nitrogen fixation. The absence of inorganic fertiliser addition to the pastureland
386 above the cave site precludes this source as a contributor to the drip water nitrogen signal. These inputs can be
387 expected to support end member isotopic compositions in the following range: Atmospheric wet deposition
388 δ¹⁵NNO₃ and δ¹⁵NNH₄ = -15‰ to +15‰ (Kendall et al., 2007), δ¹⁸ONO₃ ~ +60‰ to +95‰ (Kendall et al. 2007);
389 Manure-derived δ¹⁵N_{total} = -2.8‰ to +45.2‰ (Chalk et al., 2019 and references therein); Fixed N₂ (δ¹⁵N_{fixation}) =
390 0‰ +/- 2‰ (Casciotti, 2009 and references therein). The cave drip water nitrate composition reflects this balance
391 of inputs, albeit tempered by biogeochemical processes comprising ammonia volatilisation, assimilation into the
392 organic phase, soil mineralisation and nitrification. The inorganic dissolution of karst bedrock within the vadose
393 zone and physical processes of hydrological mixing and storage will also cause the dripwater nitrate composition
394 to deviate from input signatures.

395 Concentrations of nitrate within cave drip and pool waters are elevated relative to input rainfall. Element ratios to
396 chloride and δ¹⁸O/DH₂O isotopic signatures from other cave sites within the region have indicated the majority of
397 cave water recharge to be restricted to the winter season and the effects of evapocentration on cave drip water
398 chemistry to be limited (Smith et al., 2016b; Deeprise, 2018). Translating the assumption of limited evapo-
399 concentration affecting cave drip water chemistry to Cueva-cubío del Llanío, alongside a limited input of N from
400 bedrock dissolution, dripwater nitrogen composition appears to be a product of mixing between direct input of
401 rainfall through the karstic system and leaching of soil / sediment derived nitrogen. The δ¹⁵NNO₃ values of cave
402 waters are similar to those found in the soils/sediments. The dilute nature of nitrate within rainfall, and the
403 limited range of nitrogen isotopic composition between sources suggests cave waters are diluted to intermediate
404 concentrations whilst retaining an isotopic composition dominated by signatures of soil mineralisation and
405 nitrification. Due to the dominant influence of soil mineralisation and nitrification in the system, there is also an
406 almost complete absence of ammonia in the cave waters. The difference in δ¹⁵NNO₃ composition between the two
407 cave chambers (Figure 3), likely reflects the source of nitrogen subsequently undergoing soil mineralisation and
408 nitrification. Intensively managed pasture above High Hopes Chamber, with application of farmyard slurry /

409 manure, delivers a cave water nitrate isotopic signature enriched in ^{15}N . Rough grazing on the steep hillside above
410 Whoopee Hall, with minimal influence from farmyard slurry / manure application produces a cave water $\delta^{15}\text{NNO}_3$
411 relatively depleted in ^{15}N .

412 The oxygen isotopic composition of nitrate within cave drip waters provides information on the presence of
413 biogeochemical cycling and the relative contribution of rainfall derived inputs. The measured $\delta^{18}\text{ONO}_3$ within
414 incoming rainfall has values typical of those reported in the literature when analysed using the same microbial
415 denitrifier method ($\sim +60\text{‰}$ to $+95\text{‰}$, Kendall et al., 2007). However, there is a large shift in isotopic composition
416 between input rainfall and cave drip waters. Nitrate-oxygen isotopic values of cave waters range between -2.5‰
417 to $+6.0\text{‰}$. If nitrification is the sole pathway for the production of nitrate within the cave system, this should
418 produce a dripwater $\delta^{18}\text{ONO}_3$ value that ranges between -15.0‰ to -1.9‰ , assuming the following conditions: a
419 1:2 stoichiometry of atmospheric O_2 and rainfall oxygen incorporation into newly formed nitrate molecules;
420 assumed values of $+23.5\text{‰}$ for atmospheric O_2 (Kroopnick and Craig, 1972); a measured rainfall $\delta^{18}\text{OH}_2\text{O}$ range of
421 $+0.2\text{‰}$ to -11.2‰ within the Matienzo-Riaño region between 2011-2019; and experimentally derived
422 fractionation factors during ammonia oxidation (Casciotti et al., 2010) and oxidation of nitrite to nitrate
423 (Buchwald and Casciotti 2010). However, dripwater $\delta^{18}\text{ONO}_3$ signatures from both chambers exceed that expected
424 when assuming nitrification to be the sole production pathway (Figure 3). Where dripwater $\delta^{18}\text{ONO}_3$ exceeds the
425 upper limit of this range, further fractionation or mixing with additional nitrate source materials may be invoked.
426 In the present cave environmental setting where redox conditions are well-oxygenated and microbial
427 denitrification is deemed not to be present, we consider mixing with rainfall-derived (atmospheric) nitrate
428 enriched in ^{18}O to be responsible for the excursion of values above the maximum calculated threshold.

429

430 This partial direct transit of nutrients into cave systems has also been observed as part of the sulphur
431 biogeochemical cycle, where either excessive atmospheric deposition of pollutant derived sulphur enabled a
432 direct transfer into the cave dripwaters under a diminished significance of biogeochemical cycling (Wynn et al.,
433 2013), or an ephemeral fracture flow system allowed the rapid transport of meteoric water through the karst
434 with limited storage and mixing en-route. Even though all drip sites at Cueva-cubío del Llanío in both High Hopes
435 Chamber and Whoopee Hall are well-homogenised in both nitrate concentration and isotopic composition,
436 representing a large degree of storage and mixing of water sources within the matrix of the epikarst aquifer, a
437 proportion of fracture flow can be expected after heavy rainfall events. It is thus suspected the origin of the
438 $\delta^{18}\text{ONO}_3$ which lies above the calculated threshold value for nitrification, are due to a proportion of meteoric
439 water being delivered to the drip sites according to site specific karst hydrological characteristics. The proportion
440 of sources contributing to drip waters within each cave chamber has been parameterised using a Bayesian
441 isotope mixing model (Table 4). Within High Hopes chamber, drips fed from ephemeral fracture pathways
442 (labelled 'Fast drips 1 and 2 in Table 1), comprise 49.8% (5.4% 1SD) of nitrate sourced from manure, whilst the re-
443 mineralisation of fixed N_2 and/or the nitrification of rainfall-derived ammonia contributes 36.6% (5.4% 1SD) and
444 the remaining signal 13.6% (0.9% 1 SD) is derived from the direct contribution of nitrate contained within rainfall.
445 Within the same chamber, drip sites fed by a matrix-controlled hydrological pathway (High Hopes drips 1-6)
446 support a greater proportion of nitrate sourced from the direct contribution of rainfall (16.1%, 0.8% 1SD). In the
447 cave waters from Whoopee Hall, cave waters fed from ephemeral fracture pathways (Whoopee pool) comprise
448 just 33% (5% 1SD) of nitrate sourced from manure, whilst 54.9% (5.1% 1SD) of nitrate is sourced from the re-
449 mineralisation of fixed N_2 and/or the nitrification of rainfall-derived ammonia, and 12.2% (1.1% 1SD) sourced
450 from the direct entry of rainfall derived nitrate. Matrix-controlled pathways within Whoopee Hall (Whoopee Drip)
451 contain 14.7% (1.3% 1SD) of nitrate derived from the direct entry of rainfall. Mixing models thus support the
452 contention that cave waters in High Hopes chamber convey a greater proportion of nitrate sourced from manure.
453 They also demonstrate cave waters fed by ephemeral or fracture flow characteristics contain a lower proportion
454 of nitrate sourced from the direct entry of rainfall, thus indicating fracture pathways to convey a greater
455 proportion of water which is sourced from the base of the soil zone, compared to matrix-fed drips within the
456 same chamber. It is therefore the nutrient status of the cave surface ecosystem, as well as the nature of the land

457 surface inputs and cave system hydrology that work in concert to drive the isotopic composition of the product
458 dripwaters. Input management, soil biogeochemical processing and Epikarst hydrology, thus all appear to be
459 controlling agents of dripwater nitrate composition.

460

461 **5.2 Transfer of drip water nitrate into the speleothem record at Cueva-cubío del Llanío**

462 The concentration and isotopic composition of nitrate within speleothem calcite has great potential to inform on
463 past groundwater nitrate dynamics. However, this is dependent upon nitrate partitioning and isotopic
464 fractionation between cave drip water and associated speleothem carbonate being quantified.

465 The nitrate concentrations contained within modern speleothem carbonates from Cueva-cubío del Llanío range
466 between 0.05 to 0.37 mM NO₃. Partitioning between dripwater and speleothem carbonate causes an offset in the
467 nitrate concentration between aqueous to solid phase. Field based partition coefficients are calculated and
468 presented within Table 2. Values of DNO₃ (x 10⁻⁵) represent a relative efficiency of incorporation into
469 contemporary speleothem calcite, ranging between 0.06 to 0.42 for the replacement of carbonate with nitrate,
470 with no perceived difference between cave chambers. Compared to the partitioning of sulphate into calcite
471 (Wynn et al., 2018), where the mechanism of incorporation is assumed to follow similar principles of anion
472 substitution (Kontrec et al., 2004), the nitrate molecule represents a lower efficiency of incorporation by
473 approximately 1-3 orders of magnitude (Note the typographical error in Wynn et al., 2018 where all DSO₄ values
474 are given as x10⁵, instead of x10⁻⁵). Quantifying the efficiency of nitrate incorporation into speleothem calcite is an
475 essential first step in enabling semi-quantitative reconstruction of former nitrate loading to karst vadose zone
476 groundwater. While the mechanism of incorporation of nitrate into calcite is unresolved, we note that the
477 thermochemical radii of the CO₃²⁻ ion (0.178 nm) and NO₃⁻ (0.179 nm) are similar. Given this alone, we would
478 expect the NO₃⁻ to readily substitute for the CO₃²⁻ on lattice sites of calcite. However, any substitutions must
479 maintain overall electroneutrality i.e. balance of formal charges for the constituent ions within the crystal. The
480 substitution of NO₃⁻ therefore requires a concurrent substitution of the Ca²⁺ cation by a monovalent cation. Of the
481 alkali halides, Na⁺ and Li⁺ offer the highest possibility as their radii are either comparable (Na⁺) or smaller (Li⁺)
482 than that of Ca²⁺ (ionic radii: Ca²⁺ 0.100 nm; Li⁺ 0.760; Na⁺ 0.102 nm; K⁺ 0.138 nm) (Wiredchemist, 2021). The
483 availability of the monovalent ion in the aqueous environment is therefore expected to influence the extent of
484 substitution as reflected by the partition coefficient DNO₃, and indeed may explain, to some extent, the variation
485 in these values. Further, the partition coefficient values have a thermodynamic basis and are unlikely to define
486 the prevailing supersaturation of NO₃⁻ when calcite is being deposited. Clearly, fundamental studies are required
487 to characterise the NO₃⁻ – CO₃²⁻ substitution in calcite.

488 The isotopic composition of contemporary speleothem carbonate grown on glass plates beneath active drip sites
489 within Cueva-cubío del Llanío is presented in Figure 3 and Table 2. Values of δ¹⁵NNO₃ contained within speleothem
490 carbonate reflect closely those found within the associated cave drip waters (Figure 3). This suggests there is little
491 fractionation of δ¹⁵NNO₃ during the incorporation of nitrate into calcium carbonate and that time-resolved records
492 of speleothem carbonate would make excellent archives of changing groundwater nitrogen source. However,
493 values of δ¹⁸OONO₃ contained within speleothem carbonate appear to be of intermediate value to those found in
494 the drip waters and input rainfall. This enrichment in nitrate ¹⁸O compared to the counterpart drip waters could
495 be due to fractionation either in the laboratory or on the speleothem surface, or due to the time-integrated
496 nature of carbonate deposition (6 months duration) relative to shorter drip water collection times (approx. 24
497 hours at the drip sites of concern). Fractionation in the laboratory during sample processing would typically occur
498 during acid digestion of carbonate, whereby nitrate ions may undergo equilibrium isotopic exchange with the
499 ambient water (Kaneko and Poulson, 2013). However, despite the acidic pH during carbonate digestion, such
500 isotopic exchange is considered too slow at the low reaction temperature (room temperature) and the short
501 timescale of low pH conditions (the reaction between carbonate powder and hydrochloric acid proceeds to
502 completion to achieve a neutral pH). Fractionation on the speleothem surface could be induced if the presence of
503 nitrate assimilating bacteria specific to the cave environment caused further biogeochemical cycling and thus

504 fractionation of nitrate isotopes away from those found within the drip waters. However, if speleothem surface
505 microbes were responsible for driving isotopic enrichment in nitrate ^{18}O via assimilation, this enrichment would
506 also be expected within the cave pool waters, which contain drip waters after transit across the speleothem
507 surface and cave floor. The similarity of $\delta^{18}\text{ONO}_3$ within both drip and pool waters would seem to negate this
508 effect. We therefore consider the time-integrated nature of speleothem carbonate deposition (6 months) relative
509 to drip water collection (24 hours at the drip sites of concern) to be the main contributing factor to nitrate ^{18}O
510 enrichment. Over a growth period of 6 months, carbonate deposition will integrate dripwater nitrate sourced
511 predominantly from the well-mixed groundwater store, sporadically over-printed by short lived fracture flow
512 events during rainfall, delivering atmospheric nitrate enriched in ^{18}O which hasn't undergone any prior
513 biogeochemical modification in the soil and epikarst. Bayesian mixing models parameterise the proportion of
514 rainfall nitrate in contemporary speleothem calcite to range between 31.1% (4.7% 1 SD) for Whoopee Hall to
515 42.1% (2.7% 1SD) of the total nitrate signature in High Hopes chamber (Table 4).

516

517 **5.3. Transfer of drip water nitrate into speleothem records from other cave sites**

518 Nitrate concentrations and isotopes extracted from speleothems grown in cave sites where intensive nitrogen
519 biogeochemical monitoring of the contemporary system has not been undertaken, are used to demonstrate the
520 ubiquitous presence of nitrate within speleothem carbonate and its utility in resolving the nitrogen status of the
521 formation drip/vadose zone water. Nitrate concentration, $\delta^{15}\text{NNO}_3$ and $\delta^{18}\text{ONO}_3$ was extracted from the outer
522 growth layers of archived speleothem samples collected from Browns Folly Mine, Somerset, UK (Baker et al.,
523 1998) and Merc-1, Ethiopia (Baker et al., 2007; Asrat et al., 2008), or from modern carbonate precipitate collected
524 on glass plates beneath active drip sites at Cueva de las Perlas, Matienzo, N. Spain (Deeprise, 2018) and Pooles
525 Cavern, Derbyshire, UK. Material of indeterminate age (albeit certainly pre-anthropogenic) was also drilled from
526 the base of speleothem Ease Gill 1, Yorkshire Dales, UK (Table 3). Concentrations of nitrate present within
527 speleothem calcite depict a broad range (0.02 to 0.86 mM), with the greatest concentrations present within
528 Ethiopian sample (Merc-1). Where concentrations of nitrate have been monitored in both drip waters and coeval
529 speleothem calcite, values of DNO_3 are calculated. These are presented as $\text{DNO}_3 \times 10^{-5} = 0.11$ for Merc-1 and
530 $\text{DNO}_3 \times 10^{-5} = 0.45$ for Cueva de las Perlas (Table 2). Efficiency of nitrate incorporation into speleothem calcite thus
531 appears to be within a similar range of values to those observed within Cueva-cubío del Llanío, confirming the
532 utility of DNO_3 beyond an individual set of cave environmental conditions. The data presented (Figure 4) depict a
533 narrow range of $\delta^{15}\text{NNO}_3$ values, but a range of $\delta^{18}\text{ONO}_3$ which is broader than that discovered in Cueva-cubío del
534 Llanío, N. Spain. Speleothem Ease Gill-1 supports nitrate sourced from a dominant rainfall end-member. The pre-
535 anthropogenic calcite sourced from the base of this formation precludes the presence of inorganic fertilisers and
536 extensive manure sources. Both $\delta^{15}\text{NNO}_3$ and $\delta^{18}\text{ONO}_3$ therefore place the nitrate source firmly as atmospheric
537 deposition, which enters into the cave system without any biogeochemical cycling to re-set the oxygen isotopic
538 value. Speleothem Merc-1, from Rukiesa cave, Mechara, Ethiopia, supports a $\delta^{15}\text{NNO}_3$ isotopic composition which
539 places the nitrogen source at the boundary between manure and inorganic fertiliser. The $\delta^{18}\text{ONO}_3$ signatures from
540 two separate drill aliquots range from +6.0 to +14.5‰. The intensively cultivated area above the caves and
541 greatest concentration of nitrate recorded in speleothem calcite to date (Table 3) would seem to support an
542 inorganic ammonia and nitrate fertilizer origin), with the former being mineralised prior to incorporation into the
543 stalagmite calcite. A proportion of atmospheric nitrate entering into the cave without prior biogeochemical
544 modification is consistent with $\delta^{18}\text{ONO}_3$ above the maximum calculated threshold for nitrification and a fracture
545 flow component delivering meteoric water observed at this site (Asrat et al., 2008). Other speleothem samples
546 tested (Cueva de las Perlas, Matienzo, N. Spain; Pooles Cavern, Derbyshire, UK; Browns Folly Mine, Somerset, UK)
547 all represent modern deposition within cave sites beneath scrubland with low intensity grazing, or woodland
548 established within the last 100 years. The $\delta^{15}\text{NNO}_3$ values of all three sites fall within the overlapping source range
549 of rainfall, manure-N and inorganic ammonia fertiliser. The overlying vegetation would largely preclude any
550 organic or inorganic fertiliser input, suggesting a natural soil derived nitrogen, ultimately derived from
551 atmospheric deposition and nitrogen fixation to be the main source of nitrogen in drip waters and speleothem

552 calcite. Values of $\delta^{18}\text{ONO}_3$ in the same samples lie beyond the expected range for microbial nitrification,
553 suggesting a proportion of nitrogen deposition must be as atmospheric nitrate which enters directly into the cave
554 drip waters without prior biogeochemical modification in the soil zone.

555 Speleothem carbonate thus seems to reflect the isotopic composition of vadose zone nitrate, but which demands
556 the dual isotopic analysis of $\delta^{15}\text{NNO}_3$ and $\delta^{18}\text{ONO}_3$ to enable both source and biogeochemical modification to be
557 detected. As atmospheric nitrate also supports a mass independent excess of ^{17}O over that expected from ^{18}O
558 ($\Delta^{17}\text{O}$) (eg. Michalski et al., 2003), which is inherited through atmospheric reaction with ozone, we propose the
559 use of nitrate $\Delta^{17}\text{O}$ in addition to $\delta^{15}\text{N}$ and $\delta^{18}\text{O}$ as a tracer of atmospheric nitrate deposition entering into the
560 cave / groundwater system without prior biogeochemical modification (cf. Dietzel et al., 2014).

561

562 **Conclusions**

563 The potential for speleothem carbonate to accurately record signals of vadose zone nitrate which extend prior to
564 the era of groundwater monitoring is dependent upon understanding the impact of biogeochemical cycling, karst
565 hydrological dynamics and partitioning, upon signal integrity. Within cave waters, measurements of $\delta^{15}\text{NNO}_3$
566 demonstrate source characteristics of input nitrogen to be well preserved throughout the soil and epikarst
567 biogeochemical cycle. Values of $\delta^{18}\text{ONO}_3$ within dripwaters provide a deeper insight into biogeochemical
568 processing and hydrological dynamics, highlighting the importance of atmospheric nitrate deposition entering
569 directly through the karst without prior biogeochemical modification. Both biogeochemical cycling and
570 hydrological dynamics work in concert to determine the characteristics of dripwater nitrate entering into the cave
571 system. Across the dripwater-contemporary carbonate interface, partitioning controls the concentration of
572 nitrate incorporated into the speleothem record in a quantifiable manner and the speleothem isotopic record
573 seems unaffected by fractionation between phases. $\delta^{15}\text{NNO}_3$ within speleothem carbonate is thus deemed an
574 excellent indicator of source, whilst $\delta^{18}\text{ONO}_3$ within carbonate provides a sensitive indicator of karst hydrological
575 dynamics and biogeochemical processing. On the basis of nitrate isotope systematics established within
576 contemporary speleothem calcite, application to age-constrained records which extend throughout the
577 anthropogenic era promise an exciting development in the ability to trace vadose zone pollution dynamics. Of
578 specific interest is the ability to establish a baseline pollution status to contextualise current levels of nitrate
579 inputs, to determine nitrate retention (legacy) dynamics through the direct comparison of input records and
580 speleothem concentration profiles, and the opportunity to trace inputs to source using stable isotopes.
581 Parameterisation of vadose zone nitrate dynamics in this way is also important for the refinement of karst
582 hydrological models which are currently in a limited state of development for the prediction of nitrate
583 groundwater quality within karst.

584

585 **Figures**

586 Figure 1: Cave plan for Cueva-cubío del Llanío, Matienzo, N. Spain.

587 Figure 2: Nitrogen concentration and isotope composition of cave waters, rainfall and soil/sediment in the Cueva-
588 cubío del Llanío system.

589 Figure 3: Nitrate isotope composition of cave waters, rainfall and contemporary speleothem calcite in Cueva-
590 cubío del Llanío.

591 Boxes defining the expected range of values for $\delta^{15}\text{NNO}_3$ obtained from the mineralisation/nitrification of manure,
592 inorganic fertiliser and rainfall ammonia are sourced from Kendall et al. (2007). The range in $\delta^{15}\text{NNO}_3$ expected
593 from rainfall represent those values obtained only through the microbial denitrifier method (Kendall et al., 2007).
594 The expected range in $\delta^{15}\text{NNO}_3$ obtained from the re-mineralisation and nitrification of Fixed N_2 is presented
595 assuming minimal fractionation from source organic matter. The expected range in $\delta^{18}\text{ONO}_3$ values obtained

596 during mineralisation/nitrification have been calculated using fractionation factors developed through Casciotti et
597 al., 2007, Casciotti et al., 2010, Casciotti and Buchwald, 2010, and values of rainfall $\delta^{18}\text{O}_{\text{H}_2\text{O}}$ specific to Matienzo
598 between 2011-2019 (see data repository for full compilation of values).

599

600

601 Figure 4: Nitrate isotope composition of speleothem calcite deposited within shallow cave systems beneath
602 contrasting surface vegetation characteristics.

603 Boxes defining the expected range of values for $\delta^{15}\text{NNO}_3$ obtained from the mineralisation/nitrification of manure,
604 inorganic fertiliser and rainfall ammonia are sourced from Kendall et al. (2007). The range in $\delta^{15}\text{NNO}_3$ expected
605 from rainfall represent those values obtained only through the microbial denitrifier method (Kendall et al., 2007).
606 The expected range in $\delta^{15}\text{NNO}_3$ obtained from the re-mineralisation and nitrification of Fixed N_2 is presented
607 assuming minimal fractionation from source organic matter. The expected range in $\delta^{18}\text{ONO}_3$ values obtained
608 during mineralisation/nitrification have been calculated using fractionation factors developed through Casciotti et
609 al., 2007, Casciotti et al., 2010, Casciotti and Buchwald, 2010, and values of rainfall $\delta^{18}\text{O}_{\text{H}_2\text{O}}$ specific to each cave
610 site. For cave sites in the Matienzo locale, rainfall $\delta^{18}\text{O}_{\text{H}_2\text{O}}$ specific to Matienzo between 2011-2019 have been
611 used. For Rukiesa cave, Ethiopia, rainfall $\delta^{18}\text{O}_{\text{H}_2\text{O}}$ was obtained from the Global Network of Isotopes in
612 Precipitation (GNIP) database for Addis Ababa between 1961 to 2016. For UK cave sites, rainfall $\delta^{18}\text{O}_{\text{H}_2\text{O}}$ was
613 obtained from the GNIP database for Wallingford, UK between 1979 to 2015 (IAEA/WMO, 2020).

614 Figure S1: Rainfall and drip water discharge records at Cueva-cubío del Llanío, collected between January 2018 to
615 September 2019.

616 Figure S2: Monthly water excess between January 2018 to September 2019 for the Cueva-cubío del Llanío region.

617

618 Tables

619 Table 1: Summary data for cave waters, rainfall, soils/sediments and vegetation at Cueva-cubío del Llanío.

620 Table 2: Calculated partition co-efficients between cave waters and speleothem calcite at Cueva-cubío del Llanío.

621 Table 3: Nitrate isotope characteristics of speleothem deposits growing within cave systems which support a
622 variety of surface vegetation characteristics.

623 Table 4: Summary modelling statistics (Mean \pm 1SD) for Bayesian isotope mixing (MixSIAR) presented as
624 proportional contributions (%) of nitrate sources into cave water and contemporary speleothem deposits. Nitrate
625 sources include (1) manure nitrate, (2) Nitrification of rainfall ammonia and/or re-mineralisation of fixed N_2 , and
626 (3) direct input of rainfall nitrate.

627

628 Data availability

629 The underlying data pertaining to figures and tables is available from
630 <http://dx.doi.org/10.17635/lancaster/researchdata/xxx>.

631

632 Declaration of interests

633 The authors declare no known competing financial interests.

634

635

636 **Acknowledgements**

637 This work was supported by the UK Natural Environment Research Council (NERC) National Environmental
638 Isotope Facility (NEIF) (Grant LSMSF\CEH\L\125\11\2018), and Lancaster University. Thanks are expressed to Dr. A
639 Smith of the British Geological Survey, the British Cave Research Association Cave Science Centre and the staff at
640 Pooles Cavern, UK for enabling access to the cave and allowing monitoring activities to be undertaken. Access to
641 speleothem samples previously collected from Browns Folly Mine, UK and Rukiesa Cave, Ethiopia was obtained
642 with kind permission from Prof. A. Baker (University of New South Wales, Australia), and Prof. A. Asrat (Addis
643 Ababa University, Ethiopia). We are also grateful for the kind permission from Dr. Laura Deepprose (formerly of
644 Lancaster University) to use cave monitoring data and modern speleothem calcite collected as a part of her
645 unpublished doctorate research thesis. Mr. D. Hughes is thanked for his work in the Lancaster Environment
646 Centre Stable Isotope Laboratory. The Cantabrian government and the Matienzo caves Project provided access to
647 the cave site and provided invaluable assistance with logistical support and sample collection, for which we are
648 extremely grateful.

649

650 **Bibliography**

- 651 Aranburu, A., Arriolabengoa, M., Iriarte, E., Giralt, S., Yusta, I., Martínez-Pillado, V., Val, M. Moreno, J. and
652 Jimenez-Sanchez, M. 2015. Karst landscape evolution in the littoral area of the Bay of Biscay (north Iberian
653 Peninsula). *Quaternary International*, 364, 217-230. Doi: 10.1016/j.quaint.2014.09.025
- 654
- 655 Ascott, M.J., Goody, D.C., Wang, L., Stuart, M.E., Lewis, M.A., Ward, R.S. and Binley, A.M. 2017. Global patterns of
656 nitrate storage in the vadose zone. *Nature Communications*, 8, 1416. Doi: 10.1038/s41467-017-01321-w
- 657
- 658 Asrat A., Baker A., Umer MM., Leng MJ., Van Calsteren., P. and Smith C. 2007. A high-resolution multi-proxy
659 stalagmite record from Mechara, Southeastern Ethiopia: palaeohydrological implications for speleothem
660 palaeoclimate reconstruction. *Journal of Quaternary Science*, 22, 53–63. Doi: 10.1002/jqs.1013
- 661
- 662 Asrat, A., Baker, A., Leng, M.J., Gunn, J. and Umer, M. 2008. Environmental monitoring in the Mechara caves,
663 Southeastern Ethiopia: implications for speleothem palaeoclimate studies. *International Journal of Speleology*, 37
664 (3) 207-220.
- 665
- 666 Baker, A., Genty, D., Dreybodt, W., Barnes, W., Mockler, N and Grapes, J. (1998) Testing theoretically predicted
667 stalagmite growth rate with recently annually laminated samples: Implications for past stalagmite deposition.
668 *Geochimica et Cosmochimica Acta*, 62, 393-404.
- 669
- 670 Baker, A. and Genty, D. 1999. Fluorescence wavelength and intensity variations of cave waters. *Journal of*
671 *Hydrology*, 217, 19-34.
- 672
- 673 Baker, A., Mockler, N., and Barnes, W. 1999a. Fluorescence intensity variations of speleothem forming
674 groundwaters: Implications for paleoclimate reconstruction. *Water Resources Research*, 35, 407-413.
- 675
- 676 Baker, A, Proctor, C J and Barnes, W L, 1999b. Variations in stalagmite luminescence laminae structure at Poole's
677 Cavern, England, AD 1910–1996: calibration of a palaeoprecipitation proxy. *Holocene*, Vol.9, 683–688.
- 678
- 679 Baker, A., Asrat, A., Fairchild, IJ., Leng, M.J., Wynn, P.M., Bryant, C. Genty, D. and Umer, M. (2007) Analysis of the
680 climate signal contained within $\delta^{18}\text{O}$ and growth rate parameters in two Ethiopian stalagmites. *Geochimica et*
681 *Cosmochimica Acta*. 71, 2975-2988. Doi:10.1016/j.gca.2007.03.029
- 682

683 Baldini, J. (2001) Morphological and dimensional linkage between recently deposited speleothems and drip water
684 from Browns Folly Mine, Wiltshire, England. *Journal of Cave and Karst Studies*, 63: 83-90.
685

686 Baldini, J.U.L, McDermott, F., Baker, A., Baldini, L.M., Matthey, D.P and Railsback., L.B. (2005) Biomass effects on
687 stalagmite growth and isotope ratios: A 20th century analogue from Wiltshire, England. *Earth and Planetary*
688 *Science Letters*, 240, 486-494. Doi: 10.1016/j.epsl.2005.09.022
689

690 Buchwald, C. and Casciotti, K.L. 2010. Oxygen isotopic fractionation and exchange during bacterial nitrite
691 oxidation. *Limnology and Oceanography*, 55 (3) 1064-1074. doi:10.4319/lo.2010.55.3.1064
692

693 Cameron, K.C., Di, H.J. and Moir, J.L. 2013. Nitrogen losses from the soil/plant system: a review. *Annals of Applied*
694 *Biology*, 162, 145-173. doi:10.1111/aab.12014
695

696 Casciotti, K.L., Sigman, D.M., Hastings, M.G., Böhlke, J.K. and Hilkert, A. 2002. Measurement of the oxygen
697 isotopic composition of nitrate in seawater and freshwater using the denitrifier method. *Annals of Chemistry*, 74,
698 4905-4912. Doi: 10.1021/ac020113w
699

700 Casciotti, K.L., Sigman, D.L. and Ward, B.B. 2003. Linking Diversity and Stable Isotope Fractionation in Ammonia-
701 Oxidizing Bacteria, *Geomicrobiology Journal*, 20:4, 335-353. Doi: 10.1080/01490450390241035
702

703 Casciotti, K.L., Böhlke, J.K., McIlvin, M.R., Mroczkowski, S.J. and Hannon, J.E. 2007. Oxygen Isotopes in Nitrite:
704 Analysis, Calibration, and Equilibration. *Annals of chemistry*, 79, 2427-2436. Doi: 10.1021/ac061598h
705

706 Casciotti, K.L. 2009. Inverse kinetic isotope fractionation during bacterial nitrite oxidation. *Geochimica et*
707 *Cosmochimica Acta*, 73, 2061- 2076. Doi:10.1016/j.gca.2008.12.022
708

709 Casciotti, K.L., McIlvin, M., and Buchwald, C. 2010. Oxygen isotopic exchange and fractionation during bacterial
710 ammonia oxidation. *Limnology and Oceanography*, 55 (2) 753-762.
711

712 Chalk, P.M., Inácio, C.T. and Chen, D. 2019. An overview of contemporary advances in the usage of ¹⁵N natural
713 abundance ($\delta^{15}\text{N}$) as a tracer of agro-ecosystem N cycle processes that impact the environment. *Agriculture,*
714 *Ecosystems and Environment*, 283, 106570. Doi: 10.1016/j.agee.2019.106570
715

716 Deepprose, L.M.C. 2018. *Speleothem Climate Capture of the Neanderthal demise*. PhD, Lancaster University.
717

718 Dewit, J., Foubert, A., Desouky, H.A., Muchez, P., Hunt, D., Vanhaecke, F. and Swennen, R. 2014. Characteristics,
719 genesis and parameters controlling the development of a large stratabound HTD body at Matienzo (Ramales
720 Platform, Basque-Cantabrian Basin, northern Spain). *Marine and petroleum Geology*, 55, 6-25. Doi:
721 10.1016/j.marpetgeo.2013.12.021
722

723 Dietzel, M., Leis, A., Abdalla, R., Savarino, J., Morin, S, Böttcher, M.E. and Köhler, S. 2014. ¹⁷O excess traces
724 atmospheric nitrate in paleo-groundwater of the Saharan desert. *Biogeosciences*, 11, 3149- 3161.
725 Doi:10.5194/bg-11-3149-2014
726

727 Evans, D.R. 2001. Physiological mechanisms influencing plant nitrogen isotope composition. *Trends in plant*
728 *science*, 6 (3)
729

730 Fairchild, I.J., Tuckwell, G.W., Baker, A and Tooth, A.F. 2006. Modelling of drip water hydrology and
731 hydrogeochemistry in a weakly karstified aquifer (Bath, UK): Implications for climate change studies. *Journal of*
732 *Hydrology*, **321**, 213-231. Doi:10.1016/j.jhydrol.2005.08.002
733

734 Fairchild, I.J. and Treble, P.C. 2009. Trace elements in speleothems as recorders of environmental change.
735 Quaternary Science Reviews, 28, 449-468. Doi: 10.1016/j.quascirev.2008.11.007

736

737 Ford, D.C and Williams, P. Karst Hydrogeology and geomorphology. Wiley (2013).
738

739 Galloway, J.N., Townsend, A.R., Erismann, J.W., Bekunda, M., Cai, Z.C., Freney, J.R., Martinelli, L.A., Seitzinger, S.P.
740 and Sutton, M.A. 2008. Transformation of the nitrogen cycle: Recent trends, questions, and potential solutions.
741 Science, 320, 889-892.
742

743 Galloway, J.N., Townsend, A.R., Erismann, J.W., Bekunda, M., Cai, Z., Freney, J.R., Martinelli, L.A., Seitzinger, S.P.
744 and Sutton, M.A. 2008. Transformation of the nitrogen cycle: Recent trends, questions, and potential solutions.
745 Science, 320 (5878) 889-892. Doi: 10.1126/science.1136674.

746

747 Gutiérrez, J. 2010. Geological map of Matienzo, Arredondo, Ogarrio and surroundings. In: Corrin, J., and Smith, P.
748 (eds.) *Matienzo 50 years of speleology*. Bacup: Matienzo Caves.
749

750 Hartland, A., Fairchild, I.J., Lead, J.R., Borsato, A., Baker, A., Frisia, S., Baalousha, M. 2012. From soil to cave:
751 transport of trace metals by natural organic matter in karst drip waters. *Chem. Geol.*, **304**, 68-82. Doi:
752 10.1016/j.chemgeo.2012.01.032
753

754 Hartland A., Fairchild, I.J., Lead, J.R., Zhang, H. and Baalousha, M. 2011. Size, speciation and lability of NOM-metal
755 complexes in hyperalkaline cave dripwater. *Geochimica et Cosmochimica Acta*, 75, 7533-7551
756

757 Hartland, A., Fairchild, I.J., Lead, J.R., Dominguez-Villar, D., Baker, SA., Gunn, J., Baalousha, M. and Ju-Nam, Y.
758 2010. The dripwaters and speleothems of Poole's Cavern: A review of recent and ongoing research. *Cave and*
759 *Karst Science*, 36 (2) 37-46.
760

761 Heaton, T. H. E. 1986. Isotopic studies of nitrogen pollution in the hydrosphere and atmosphere: a review.
762 *Chemical Geology*, 59, 87-102.
763

764 Högberg, P. 1997. Tansley Review No. 95. 15N natural abundance in soil-plant systems. *New Phytologist*, 137,
765 179-203
766

767 Husic, A., Fox, J., Adams, E., Backus, J., Pollock, E., Ford, W. and Agourdis, C. 2019a. Inland impacts of atmospheric
768 river and tropical cyclone extremes on nitrate transport and stable isotope measurements. *Environmental Earth*
769 *Sciences*. 78:36. Doi: 10.1007/s12665-018-8018-x
770

771 Husic, A., Fox, J., Adams, E., Ford, W., Agourdis, C., Currens, J. and Backus, J. 2019b. Nitrate Pathways, Processes,
772 and Timing in an Agricultural Karst System: Development and Application of a Numerical Model. *Water Resources*
773 *Research*, 55, 2079-2103. Doi: 10.1029/2018WR023703
774

775 Jiménez-Sánchez, M., Stoll, H., Vadillo, I., López-Chicano, M., Domínguez-Cuesta, M., Martín-Rosalez, W. and
776 Meléndez-Asensio, M. 2008. Groundwater contamination in caves: four case studies In Spain. *International*
777 *Journal of Speleology*, 37 (1) 53-66.
778

779 Kaneko, M. and Poulson, S.R. 2013. The rate of oxygen isotope exchange between nitrate and water. *Geochimica*
780 *et Cosmochimica Acta*, 118, 148-156. Doi: 10.1016/j.gca.2013.05.010
781

782 Kendall, C., Elliot, E.M. and Wankel, S.D. 2007. Tracing anthropogenic inputs of nitrogen to ecosystems. In:
783 Michener, R.H. and Lajtha, K. (eds.) *Stable isotopes in ecology and environmental science*. 2nd edition. Blackwell
784 publishing, p. 375-449.

785
786 Kontrec, J., Kralj, D., Brečević, L., Falini, G., Fermani, S., Noethig-Laslo, V. and Miroslavljević, K. 2004.
787 Incorporation of inorganic anions in calcite. *European Journal of Inorganic Chemistry*, 4579-4585. Doi:
788 10.1002/ejic.200400268
789
790 Kroopnick, P.M. and Craig, H.C. 1972. Atmospheric oxygen: isotopic composition and solubility fractionation.
791 *Science*, 175 (4017) 54-55. Doi: 10.1126/science.175.4017.54
792
793
794 Liu, X-Y., Koba, K., Makabe, A. and Liu, C-Q. 2014. Nitrate dynamics in natural plants: insights based on the
795 concentration and natural isotope abundances of tissue nitrate. *Frontiers in plant science*, 5, article number 355.
796 Doi: 10.3389/fpls.2014.00355
797
798 Matiatos, I., Wassenaar, L.I., Monteiro, L.R., Venkiteswaran, J.J., Gooddy, D.C., Boeckx, P., Sacchi, E., Yue, F-J.,
799 Michalski, G., Alonso-Hernández, C., Biasi, C., Bouchaou, L., Edirisinghi, N.V., Fadhullah, W., Fianko, J.R., García-
800 Moya, A., Kazakis, N., Li, S-L., Luu, M.T.N., Priyadarshane, S., Re, V., Rivera, D.S., Romanelli, A., Sanyal, P.,
801 Tamoo, F., Trinh, D.A., Walters, W., and Welti, N. 2021. Global patterns of nitrate isotope composition in rivers
802 and adjacent aquifers reveal reactive nitrogen cascading. *Communications Earth and Environment*.
803
804
805 Mayer B, Bollwerk SM, Mansfeldt T, Hütter B, Veizer J. 2001. The oxygen isotope composition of nitrate generated
806 by nitrification in acid forest floors. *Geochimica et Cosmochimica Acta*, 65, 2743–2756. Doi.org/10.1016/S0016-
807 7037(01)00612-3
808
809 Michalski, G., Scott, Z., Kabling, M and Thiemens, M.H. 2003. First measurements and modelling of $\delta^{17}\text{O}$ in
810 atmospheric nitrate *Geophysical research letters*, 30 (16), art. No-1870. Doi: 10.1029/2003GL017015
811
812 Newton, K.E., Fairchild, IJ. and Gunn, J. 2015. Rates of calcite precipitation from hyperalkaline waters, Poole's
813 Cavern, Derbyshire, UK. *Cave and Karst Science*, 42 (3) 116-124.
814
815 Romanelli, A., Soto, D.X., Matiatos, I., Martínez, D.E., Esquiú, S. 2020. A biological and nitrate isotopic assessment
816 framework to understand eutrophication in aquatic ecosystems. *Science of The Total Environment*, 715, 136909.
817 Doi: 10.1016/j.scitotenv.2020.136909
818
819 Sigman, D.M., Casciotti, K.L., Andreani, M., Barford, C., Galanter, M. and Böhlke, J.K. 2001. A bacterial method for
820 the nitrogen isotopic analysis of nitrate in seawater and freshwater. *Annals of Chemistry*, 73, 4145-4153. Doi:
821 10.1021/ac010088e
822
823 Smith, A.C., Wynn, P.M., Barker, P.A. and Leng, M.J. 2015. Drip water electrical conductivity as an indicator of
824 cave ventilation at the event scale. *Science of the total environment*, 532, 517-527. Doi:
825 10.1016/j.scitotenv.2015.06.037
826
827 Smith, A.C., Wynn, P.M., Barker, P.A., Leng, M.J., Noble, S.R. and Tych, W. 2016a. North Atlantic forcing of
828 moisture delivery to Europe throughout the Holocene. *Scientific Reports*, 6, 24745. Doi: 10.1038/srep24745
829
830 Smith, A.C., Wynn, P.M., Barker, P.A., Leng, M.J., Noble, S.R. and Stott, A. 2016b. Cave monitoring and the
831 potential for palaeoclimate reconstruction from Cueva de Asiul, Cantabria (N. Spain). *International Journal of*
832 *Speleology*, 45 (1), 1-9. Doi: 10.5038/1827-806X.45.1.1928
833
834 Soto, D.X., Koehler, G., Wassenaar, L.I., Hobson, K.A. 2019. Spatio-temporal variation of nitrate sources to Lake
835 Winnipeg using N and O isotope ($\delta^{15}\text{N}$, $\delta^{18}\text{O}$) analyses. *Sci. Total Environ.*, 647, 486–493. Doi:
836 10.1016/j.scitotenv.2018.07.346

837
838 Stock, B.C., Semmens, B.X. 2013. MixSIAR User Manual. Version 3.1. <https://github.com/brianstock/MixSIAR>.
839
840 Venkiteswaran, J.J., Boeckx, P., Goody, D.C. 2019. Towards a global interpretation of dual nitrate isotopes in
841 surface waters. *Journal of Hydrology X*, 4, 100037. Doi: 10.1016/j.hydroa.2019.100037
842
843 Vitousek, P.M., Aber, J.D., Howarth, R.W., Likens, G.E., Matson, P.A., Schindler, D.W., Schlesinger, W.H. and
844 Tilman, D.G. 1997. Technical report: Human alteration of the global nitrogen cycle: Sources and consequences.
845 *Ecological Applications*, 7 (3), 737-750.
846
847 Wang, L., Butcher, A.S., Stuart, M.E., Goody, D.C. and Bloomfield, J.C. 2013. The nitrate time bomb: A numerical
848 way to investigate nitrate storage and lag time in the unsaturated zone. *Environ. Geochem. Health*, 35, 667-681.
849 Doi: 10.1007/s10653-013-9550-y
850
851 Wells, N.S., Baisden, W.T. and Clough, T.J. 2015. Ammonia volatilisation is not the dominant factor in determining
852 the soil nitrate isotopic composition of pasture systems. *Agriculture, Ecosystems and Environment*, 199, 290-300.
853 Doi: 10.1016/j.agee.2014.10.001
854
855 Wynn, P.M., Fairchild, I.J., Baker, A., Baldini, J.U.L. and McDermott, F. 2008. Isotopic archives of sulphate in
856 speleothems. *Geochim. Cosmochim. Acta* **72**, 2465-2477. Doi:10.1016/j.gca.2008.03.002
857
858 Wynn, P.M., Borsato, A., Baker, A., Frisia, S., Miorandi, R. & Fairchild, I.J. 2013. Biogeochemical cycling of sulphur
859 in karst and transfer into speleothem archives at Grotta di Ernesto, Italy. *Biogeochemistry* **114**, 255-267. Doi:
860 10.1007/s10533-012-9807-z
861
862 Wynn, P.M., Fairchild, I.J., Borsato, A., Spötl, C., Hartland, A., Baker, A., Frisia, S. and Baldini, J.U.L. 2018. Sulphate
863 partitioning into calcite: Experimental verification of pH control and application to seasonality in speleothems.
864 *Geochimica et Cosmochimica Acta*, 226, 69-83. Doi: 10.1016/j.gca.2018.01.020
865
866 Yang, P., Wang, Y., Wu, X., Chang, L., Ham, B., Song, L. and Groves, C. 2020. Nitrate sources and biogeochemical
867 processes in karst underground rivers impacted by different anthropogenic input characteristics. *Environmental*
868 *Pollution*, 265, 114835. Doi: 0.1016/j.envpol.2020.114835
869
870 Yue, F-J., Li, S-L., Zhong, J. and Liu, J. 2018. Evaluation of Factors Driving Seasonal Nitrate Variations in Surface and
871 Underground Systems of a Karst Catchment. *Vadose Zone Journal*. 17:170071. Doi:10.2136/vzj2017.04.0071
872
873 Yue, F-J, Waldron, S., Li, S-L., Wang, Z-J., Zeng, J., Xu, S., Zhang, Z-C. and Oliver, D.M. 2019. Land use interacts with
874 changes in catchment hydrology to generate chronic nitrate pollution in karst waters and strong seasonality in
875 excess nitrate export. *Science of the Total Environment*, 696, 134062. Doi: 10.1016/j.scitotenv.2019.134062
876
877 Internet source references
878 <http://www.wiredchemist.com/chemistry/data/atomic-and-ionic-radii> (accessed 6th August 2020).
879 [Dataset] IAEA/WMO (2020). Global Network of Isotopes in Precipitation. The GNIP Database. Accessible
880 at: <http://www.iaea.org/water> (accessed 8th July 2020).
881
882
883
884

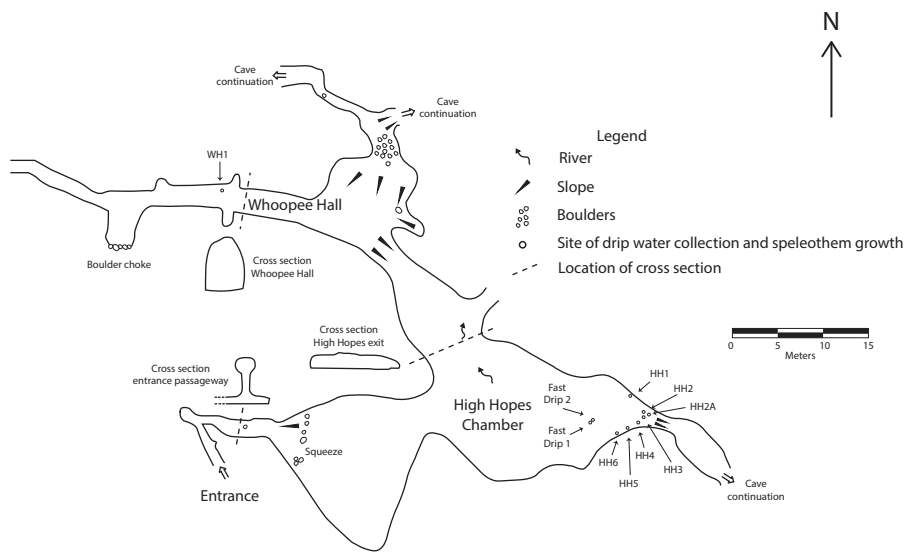
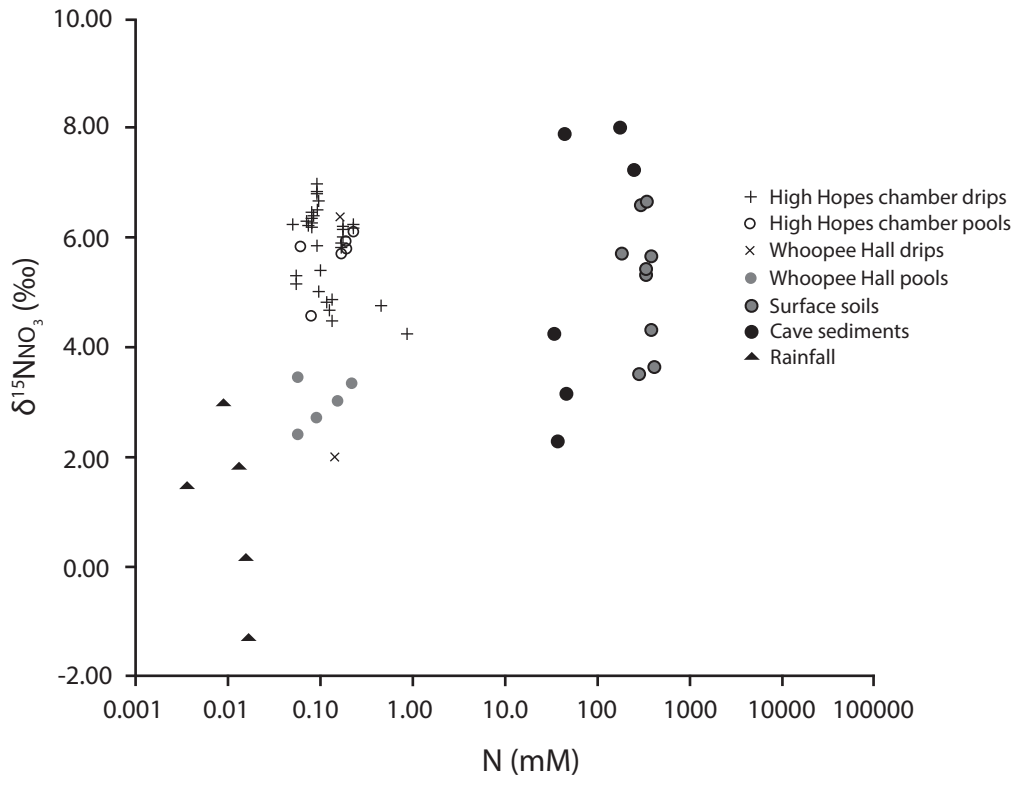
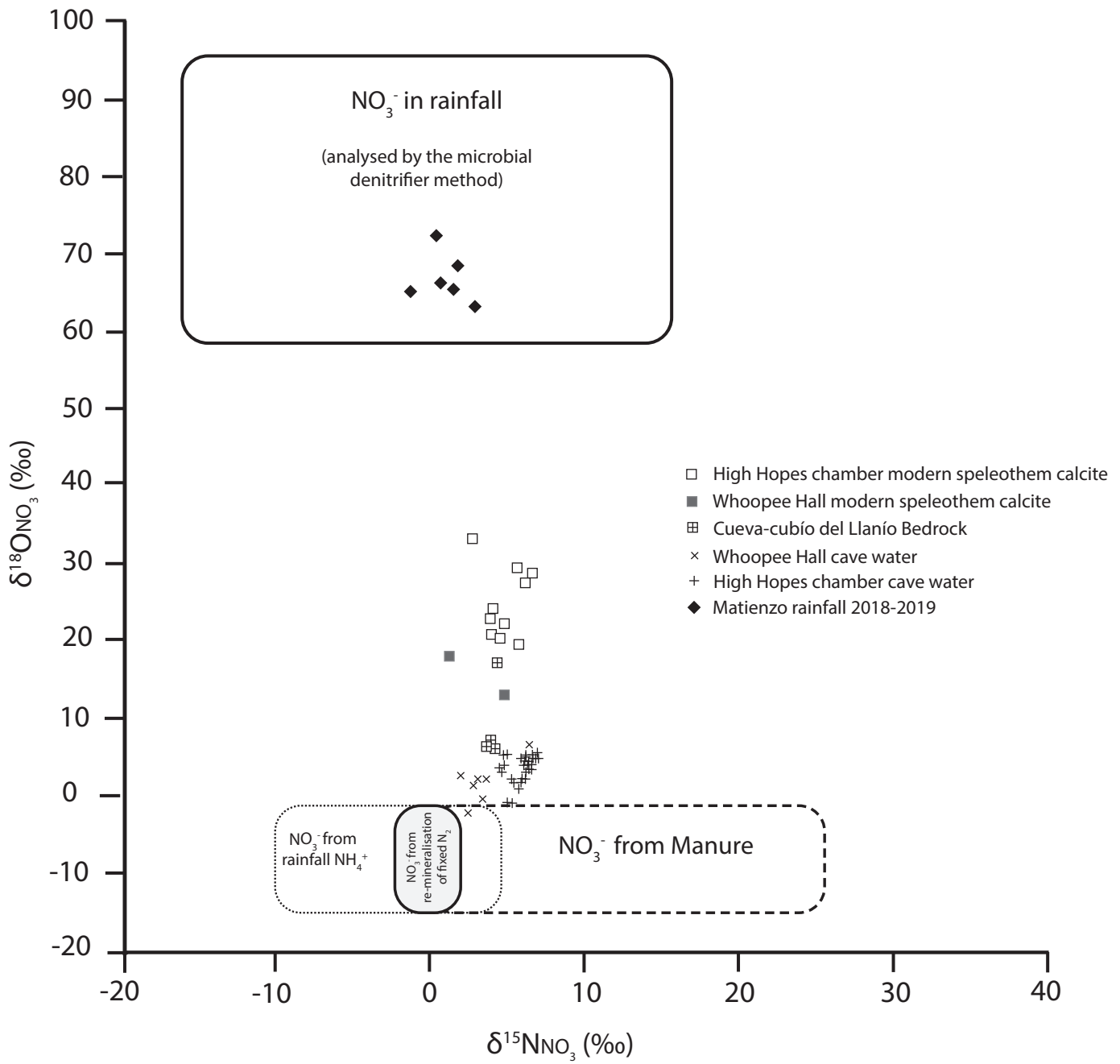
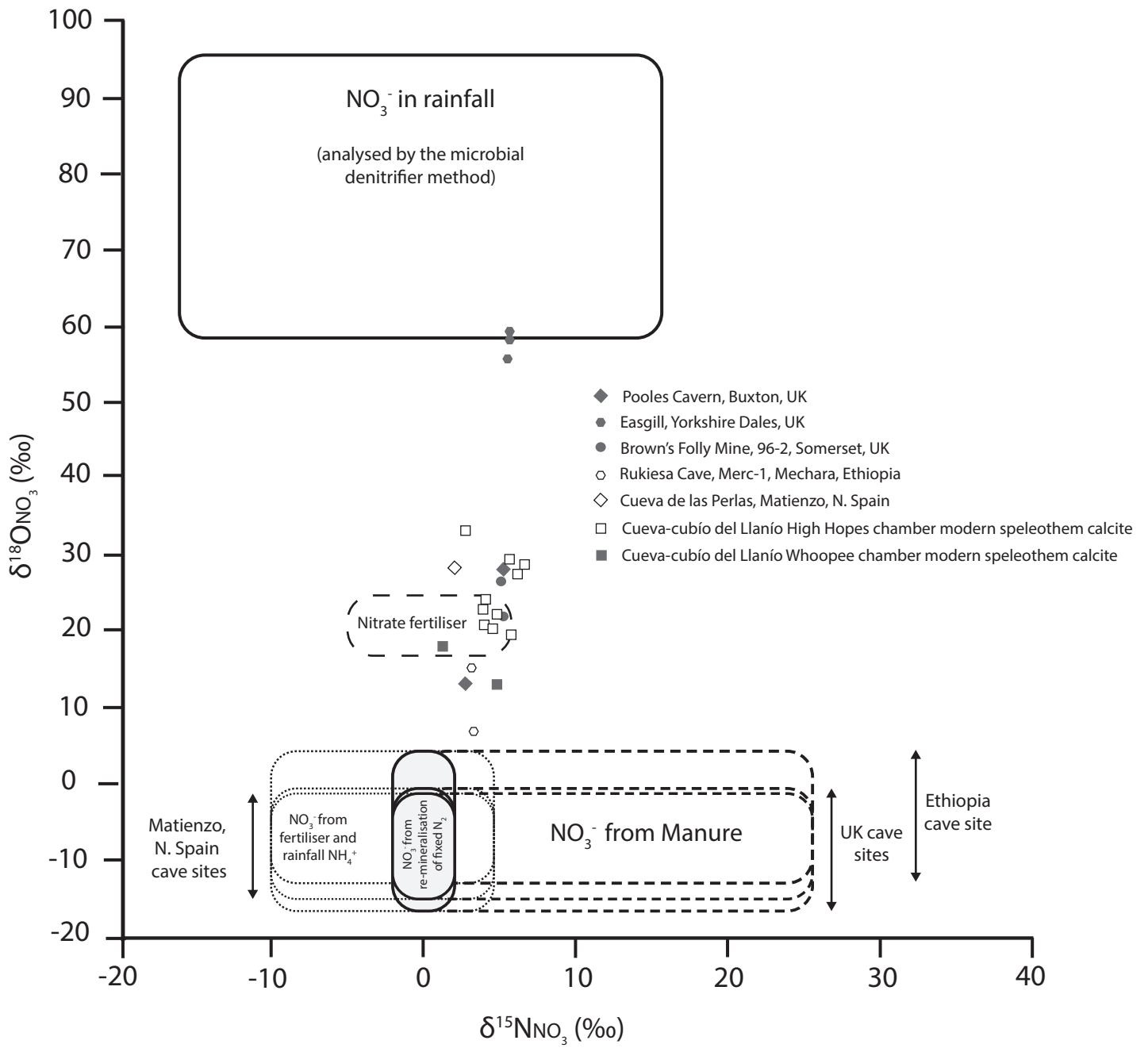


Figure 2







885
886
887
888
889
890
891
892

Table 1

Sample	pH	EC	Temp (°C)	Total alkalinity (mM CaCO ₃)	NO ₃ -N (mM)	NH ₄ -N (mM)	δ ¹⁵ NNO ₃ (‰)	δ ¹⁸ ONO ₃ (‰)
Dripwaters								
High Hopes Fast Drip 1	7.46	390	12.8	1.80	0.15	0.009	+6.0	+2.2
	n = 2	n = 2	n = 2	n = 1	n = 6	n = 1	n = 5	n = 5
	(7.14 to 7.78)	(384 to 395)	(12.5 to 13.0)		(0.05 to 0.23)		(+5.3 to +6.2)	(-1.3 to +4.7)
High Hopes Fast Drip 2	7.85	384.00	12.70	1.50	0.17	0.002	+5.9	+2.1
	n = 1	n = 1	n = 1	n = 2	n = 5	n = 1	n = 4	n = 4
				(1.24 to 1.76)	(0.05 to 0.23)		(+5.2 to +6.2)	(-1.5 to +4.4)
High Hopes 1	7.86	493	14.6	No data available	0.12	0.007	+4.7	+3.5
	n = 1	n = 2	n = 1		n = 6	n = 3	n = 4	n = 4
		(455 to 531)			(0.10 to 0.13)	(0.002 to 0.011)	(+4.5 to +4.9)	(+2.8 to +4.7)
High Hopes 2	7.97	460	12.4	1.93	0.09	0.005	+6.4	+4.0
	n = 4	n = 4	n = 3	n = 3	n = 4	n = 2	n = 5	n = 5
	(7.59 to 8.16)	(435 to 479)	(11.4 to 14.3)	(1.64 to 2.40)	(0.08 to 0.09)	(0.005 to 0.005)	(+5.3 to +7.0)	(+1.5 to +4.5)
High Hopes 2A	7.79	448	13.3	1.84	0.08	0.011	+6.5	+3.9
	n = 2	n = 3	n = 2	n = 1	n = 3	n = 2	n = 3	n = 3
	(7.62 to 7.95)	(444 to 455)	(11.8 to 14.7)		(0.08 to 0.09)	(0.004 to 0.017)	(+6.2 to +6.8)	(+3.4 to +4.8)
High Hopes 3	7.96	441	14.4	1.59	0.09	0.005	+5.9	+2.7
	n = 2	n = 3	n = 1	n = 2	n = 3	n = 2	n = 3	n = 3
	(7.87 to 8.05)	(425 to 461)		(1.48 to 1.70)	(0.08 to 0.11)	(0.005 to 0.005)	(+5.4 to +6.2)	(+1.2 to +3.5)
High Hopes 4	8.03	446	12.5	1.87	0.09	0.006	+6.1	+3.8
	n = 3	n = 4	n = 3	n = 3	n = 4	n = 2	n = 4	n = 4
	7.84 to 8.14	(435 to 458)	(11.5 to 14.2)	(1.85 to 1.88)	(0.07 to 0.10)	(0.005 to 0.008)	(+5.0 to +6.8)	(+2.8 to +4.9)
High Hopes 5	7.87	437	14.1	No data available	0.09	0.004	+6.5	+3.4
	n = 1	n = 2	n = 1		n = 3	n = 2	n = 3	n = 3
		(436 to 437)			(0.08 to 0.09)	(0.004 to 0.004)	(+6.4 to +6.8)	(+2.9 to +4.5)
High Hopes 6	8.00	436	13.0	1.88	0.09	0.004	+6.5	+4.0
	n = 2	n = 3	n = 2	n = 2	n = 3	n = 3	n = 3	n = 3
	(7.88 to 8.11)	(417 to 455)	(12.1 to 13.8)	(1.80 to 1.96)	(0.09 to 0.10)	(0.004 to 0.005)	(+6.3 to +6.6)	(+3.4 to +4.7)
Whoopee Hall 1	8.18	386	11.7	1.53	0.15	<LOD	+4.2	+4.2

	n = 2 (8.17 to 8.20)	n = 2 (359 to 413)	n = 1	n = 2 (1.40 to 1.66)	n = 2 (0.14 to 0.17)		n = 2 (+2.0 to +6.4)	n = 2 (+2.4 to +6.0)
Pool waters								
High Hopes Pools	8.10	365	11.8	1.69	0.17	0.011	+5.9	+1.7
	n = 4 7.87 to 8.20	n = 5 (344 to 382)	n = 5 (11.4 to 13.0)	n = 5 (1.64 to 1.82)	n = 6 (0.06 to 0.23)	n = 1	n = 6 (+5.8 to +6.1)	n = 6 (+0.3 to +3.8)
Whoopee Hall Pools	7.99	347	13.7	1.30	0.12	0.006	+3.0	+1.3
	n = 3 (7.89 to 8.11)	n = 5 (278 to 427)	n = 3 (12.4 to 14.4)	n = 2 (1.25 to 1.36)	n = 5 (0.06 to 0.23)	n = 4 (0.004 to 0.008)	n = 5 (+2.4 to +3.4)	n = 5 (-2.5 to +1.9)
Rain water								
Jan – April, Sept 2019	---	31	---	---	0.01	0.012	+1.0	+66.5
		n = 3 (28.0 to 70.0)			n = 7 (0.001 to 0.02)	n = 7 (0.006 to 0.021)	n = 5 (-1.3 to +3.0)	n = 5 (+62.3 to +71.9)
Vegetation								
At cave entrance	---	---	---	---	2148	---	+0.3	---
					n = 3 (2110 to 2170)		n = 3 (-1.1 to +1.0)	
Above Hope chamber	---	---	---	---	2012	---	+1.4	---
					n = 3 (1555 to 2599)		n = 3 (+0.4 to +2.3)	
Soils / sediments								
Hope chamber Surface soils	---	---	---	---	327	---	+5.9	---
					n = 6 (196 to 364)		n = 6 (+5.4 to +6.7)	
Whoopee chamber Surface soils	---	---	---	---	404.8	---	+3.8	---
					n = 3 (319.1 to 461.9)		n = 3 (+3.5 to +4.2)	
Cave sediments	---	---	---	---	72.9	---	+5.1	---
					n = 5 (35.7 to 192.9)		n = 5 (+2.3 to +8.0)	
Bedrocks								
Llanio bedrock	---	---	---	---	0.71	---	+4.5	10.81
					n = 2 (0.5 to 0.9)		n = 2 (+4.2 to +4.7)	n = 2 (+5.4 to +16.2)

893

894 Tabulated data are presented as average values, with the data range presented in parentheses. n-values vary with
895 sample site and measurement parameter, due to site specific conditions impacting sampling frequency and
896 availability of water for chemical determinands. Underlying data to tabulated summary statistics is available
897 through the data repository at <http://dx.doi.org/10.17635/lancaster/researchdata/xxx>.

898

899

Table 2

Speleothem growth site	Collection interval	Growth substrate	Dripwater pH ^a	Water Temperature (°C) ^a	Dripwater CO ₃ ²⁻ (mM) ^b	Dripwater HCO ₃ ⁻ (mM) ^b	Dripwater NO ₃ ⁻ (mM) ^c	Dripwater NO ₃ ⁻ /CO ₃ ²⁻ molar ratio ^d	NO ₃ ⁻ (mM) speleothem calcite ^e	NO ₃ ⁻ /CO ₃ ²⁻ speleothem calcite ^f	DNO ₃ CO ₃ (x10 ⁻⁵) ^g	δ ¹⁵ NNO ₃ speleo (‰) ^h	δ ¹⁸ ONO ₃ speleo (‰) ^h
Hope Chamber 2	January 2019 – August 2019	Stalagmate surface	7.93	12.4	0.020	4.12	0.09	4.24	0.1	9.98 ^{x10⁻⁶}	0.24	+6.1	+18.9
			n = 3	n = 3	n = 2	n = 2	n = 4	(3.42 to 5.34)	n = 1	(0.19 to 0.29)	n = 1	n = 1	
			(7.59 to 8.16)	(11.4 to 14.3)	(0.015 to 0.027)	(3.49 to 4.75)	(0.08 to 0.09)						
Hope Chamber 3	January 2018 – January 2019	Stalagmate surface	8.05	No data	0.013	2.93	0.11	8.3	0.08	7.56 ^{x10⁻⁶}	0.09	+4.6	+21.0
			n = 1		n = 1	n = 1	n = 1		n = 4	(4.77 ^{x10⁻⁶} to 1.13 ^{x10⁻⁵})	(0.06 to 0.14)	n = 4	n = 4
								(0.05 to 0.11)			(+4.3 to +5.3)	(+20.0 to +22.3)	
Hope Chamber 3	January 2019 – September 2019	Watch glass	7.87	14.4	0.011	3.38	0.08	7.79	0.15	1.46 ^{x10⁻⁵}	0.19	+6.4	+27.0
			n = 1	n = 1	n = 1	n = 1	n = 2	(7.50 to 8.07)	n = 1	(0.18 to 0.20)	n = 1	n = 1	
							(0.08 to 0.09)						
Hope Chamber 4	January 2019 – September 2019	Watch glass	8.03	12.5	0.016	3.71	0.09	5.38	0.12	1.23 ^{x10⁻⁵}	0.23	+4.4	+23.2
			n = 3	n = 3	n = 3	n = 3	n = 4	(4.76 to 6.73)	n = 1	(0.18 to 0.26)	n = 1	n = 1	
			(7.84 to 8.14)	(11.5 to 14.2)	(0.011 to 0.020)	(3.68 to 3.72)	(0.07 to 0.10)						
Hope Chamber 6	January 2019 – September 2019	Watch glass	8.00	13.0	0.015	3.73	0.09	6.17	0.12	1.21 ^{x10⁻⁵}	0.20	+3.3	+32.3
			n = 2	n = 2	n = 1	n = 1	n = 3	(5.60 to 6.51)	n = 1	(0.19 to 0.22)	n = 1	n = 1	
			(7.88 to 8.11)	(12.1 to 13.8)			(0.09 to 0.10)						
Whoopee Chamber 1	January 2018 – January 2019	Stalagmate surface	8.18	11.7	0.018	3.02	0.15	8.67	0.08	8.05 ^{x10⁻⁶}	0.09	+1.6	+17.2
			n = 2	n = 1	n = 2	n = 2	n = 2	(8.19 to 8.98)	n = 1	(0.09 to 0.10)	n = 1	n = 1	
			(8.17 to 8.20)		(0.016 to 0.02)	(2.77 to 3.28)	(0.14 to 0.17)						
Whoopee Chamber 1	January 2019 – August 2019	Stalagmate surface	8.17	11.7	0.016	2.77	0.14	8.98	0.37	3.74 ^{x10⁻⁵}	0.42	+5.1	+12.3
			n = 1	n = 1	n = 1	n = 1	n = 1		n = 1		n = 1	n = 1	

Merc-1 Rukiesa, Ethiopia^a	2004	Speleothem latest growth	7.81	No data	0.022	6.17	1.77	79.2	0.85	8.497 ^{x10-5}	0.11	+3.5	+10.2
			n = 8		n = 11	n = 11	n = 2	(31.7 to 300.3)	(0.841 to 0.859)	(8.41 ^{x10-5} to 8.59 ^{x10-5})	(0.03 to 0.27)	(+3.5 to +3.6)	(+6.0 to +14.5)
			(7.47 to 8.15)		(0.002 to 0.089)	(1.55 to 10.7)	(0.71 to 2.83)					n = 2	n = 2
CP1-15 Perlas, Matienzo^j	2013-2015	Watch glass	8.39	13.4	0.027	2.71	0.04	1.47	0.07	6.63 ^{x10-6}	0.45	+2.1	+28.2
			n = 12	n = 12	n = 3	n = 3	n = 4	(0.46 to 2.30)	n = 1		(0.29 to 1.43)	n = 1	n = 1
			(8.1 to 8.52)	(12.0 to 14.8)	(0.012 to 0.039)	(2.57 to 2.77)	(0.006 to 0.088)						

Tabulated data are presented as average values, with the data range presented in parentheses. See data repository for underlying analytical results. n-values vary with sample site and measurement parameter, due to site specific conditions impacting sampling frequency and availability of water for chemical determinands.

^aRange in Temp and pH reflect measured value

^bTotal inorganic carbon speciation was undertaken using PHREEQC and concentrations derived from relative activity co-efficients. The range in carbonate and bicarbonate values reflects measured alkalinity and associated sample pH unless otherwise stated.

^cRange in nitrate represents true sample values

^dRange in NO₃⁻/CO₃²⁻ ratio in drip waters reflects pairing of max and min values in each data set.

^eRange in speleothem nitrate represents replicate analyses of the same sample

^fRange in NO₃⁻/CO₃²⁻ ratio of speleothem calcite represents replicate analyses of the same sample.

^gRange in DNO₃^{x10-5} represents pairing of max and min solid and solution ratios for each sample.

^hRange in speleothem isotope values represents replicate analyses of the same sample.

ⁱpH data taken from Asrat et al., (2008). Carbonate and bicarbonate values calculated from calcium and magnesium data obtained from Asrat et al., (2008).

^jAll raw data obtained from Deeprise (2018).

Table 3

Speleothem Name	Cave details	Sample description	Year of calcite deposition	NO ₃ (mM) in speleothem carbonate	δ ¹⁵ NNO ₃ (‰)	δ ¹⁸ ONO ₃ (‰)	n =	References
MERC-1	Rukiesia cave, Ethiopia, Mercury chamber	Speleothem (surface scrape). Actively depositing when collected. Natural cave site developed within Jurassic Limestone, intercalated with marl and mudstone. Cave chamber 25 m below the surface. Overlying vegetation comprises agricultural cultivation of maize and millet following woodland clearance in the 1930's	2004	0.850 (0.841 to 0.859)	+3.5 (+3.5 to +3.6)	+10.2 (+6.0 to +14.5)	2	Asrat et al., 2007, 2008; Baker et al., 2007
BFM-96-2	Browns Folly Mine, UK	Speleothem (surface scrape). Actively depositing when collected. Building stone mine within Oolitic limestone, Somerset, UK. Mine abandoned in 1886. Overlying secondary woodland developed over the past 100 years.	1996	0.086 (0.081 to 0.090)	+5.5 (+5.4 to +5.5)	+23.6 (+21.2 to +25.9)	2	Baker et al., 1998, 1999; Baldini et al., 2001, 2005; Fairchild et al., 2006
Perlas CP1-15	Cueva Perlas, Matienzo, N. Spain	Calcite deposition on watch glass. Natural cave site with approx. 7 m overburden rock thickness, formed in a hydrothermal dolomite body within Early Cretaceous carbonate deposits. The cave site is overlain by natural grassland supporting low intensity grazing.	2013-2015	0.066	+2.1	+28.2	1	Deeprise, L. 2018
Pooles RC1	Pooles Cavern, Derbyshire, UK. Roman Chamber	Calcite deposition on watch glass beneath hyperalkaline drip site (pH = 12). Natural cave site overlain by limewaste from early 20 th C activity. Deciduous woodland forms vegetation cover since at least 1820.	June 2019	0.047	+3.1	+13.5	1	Baker and Genty, 1999; Baker et al., 1999b; Hartland et al., 2010, 2012; Newton et al., 2015
Pooles PE2	Pooles Cavern, Derbyshire, UK. Poached Egg chamber	Calcite deposition on watch glass beneath hyperalkaline drip site (pH = 10-11). Natural cave site overlain by limewaste from early 20 th C activity. Deciduous woodland forms vegetation cover since at least 1820.	June 2019	0.021	+5.3	+28.4	1	Baker et al., 1998b; Baker and Genty, 1999; Hartland et al., 2010, 2012; Newton et al., 2015
Ease Gill 1	Ease Gill caverns, Cumbria, UK	Speleothem (basal drill sample). Collected in Ease Gill Beck, abandoned away from site of growth. Natural cave site formed within Lower carboniferous limestone on the Yorkshire Dales – Cumbrian border. Overlying vegetation is natural grassland supporting low intensity rough grazing.	Pre-anthropogenic	0.186 (0.181 to 0.191)	+6.0 (+5.8 to +6.0)	+57.3 (+55.3 to +58.6)	3	No publications to date

Data values are presented as analytical averages, with ranges presented in parentheses.

Number of analyses (n =) refers to separate drill aliquots extracted from each speleothem, other than Ease Gill 1 where n represents repeat analysis of a bulk extracted powder.

Table 4

Cave Chamber	Cave water Type	Manure	Nitrification	Rainfall
High Hopes (n=15)	Fracture	49.8 ± 5.4	36.6 ± 5.4	13.6 ± 0.9
High Hopes (n=25)	Matrix	51.0 ± 5.5	32.9 ± 5.5	16.1 ± 0.8
Whoopee Hall (n=5)	Fracture	33.0 ± 5.0	54.9 ± 5.1	12.2 ± 1.1
Whoopee Hall (n=2)	Matrix	34.8 ± 5.6	50.5 ± 5.8	14.7 ± 1.3
High Hopes speleothem (n=5)	Matrix	36.2 ± 5.4	21.7 ± 5.7	42.1 ± 2.7
Whoopee Hall speleothem (n=2)	Matrix	33.3 ± 10.9	35.6 ± 11.3	31.1 ± 4.7

Supplementary information

Contemporary systematics of vadose zone nitrate capture by speleothem carbonate

Wynn P.M.^{a*}, Ambler, S.^a, Grefe I.^a, Soto D.X.^b, Surridge, B.W.J.^a, Gabitov, R.I.^c, Barker, P.A.^a, Anwar, J.^a,
Quin, A.^a, Pereira, M.G.^b and Grant H.K.^b

^a*Lancaster Environment Centre, Lancaster University, Lancaster,
LA1 4YQ, UK.*

^b *UK Centre for Ecology and Hydrology, Lancaster, LA1 4AP, UK*

^c*Department of Geosciences, Mississippi State University, Mississippi State, MS 39762, United States.*

Corresponding author. E-mail address: p.wynn@lancaster.ac.uk

Drip rate and rainfall intensity data from Cueva-cubío del Llanío

Drip rates were monitored in Cueva-cubío del Llanío using stalagmate loggers placed on top of actively depositing speleothems. Each logging device was programmed to record the number of drips every 10 mins, with data processed to represent drip discharge in millilitres per hour. The conversion from drip count to water volume assumed a volume of 0.1 ml per drop (Collister and Matthey, 2008). Rainfall was recorded using a Pluvimate logger and raingauge housing, sited in the neighbouring village of Matienzo. Rainfall was recorded as drops per 10 mins, converted to mm per hour using the conversion factor of 0.012. The record duration from each logger was dependent upon the battery life and memory capacity of each device, hence the logging hiatus between September 2018 to January 2019. Temperature was monitored external to the cave system in the neighbouring village of Matienzo, using a Tinytag Plus, TGP4017. Data were logged at one hour intervals and have an accuracy of +/- 0.01 °C.

Figure S1 presents a rainfall record collected between January 2018 to September 2019 within the neighbouring village of Matienzo, plotted against the drip rate response of three separate drip locations within Cueva-cubío del Llanío. The rainfall record shows a seasonal distribution, with maxima occurring during the winter and minima during the summer months. This distribution is consistent with more extensive records within the region (Smith et al., 2016; Deepröse et al., 2018).

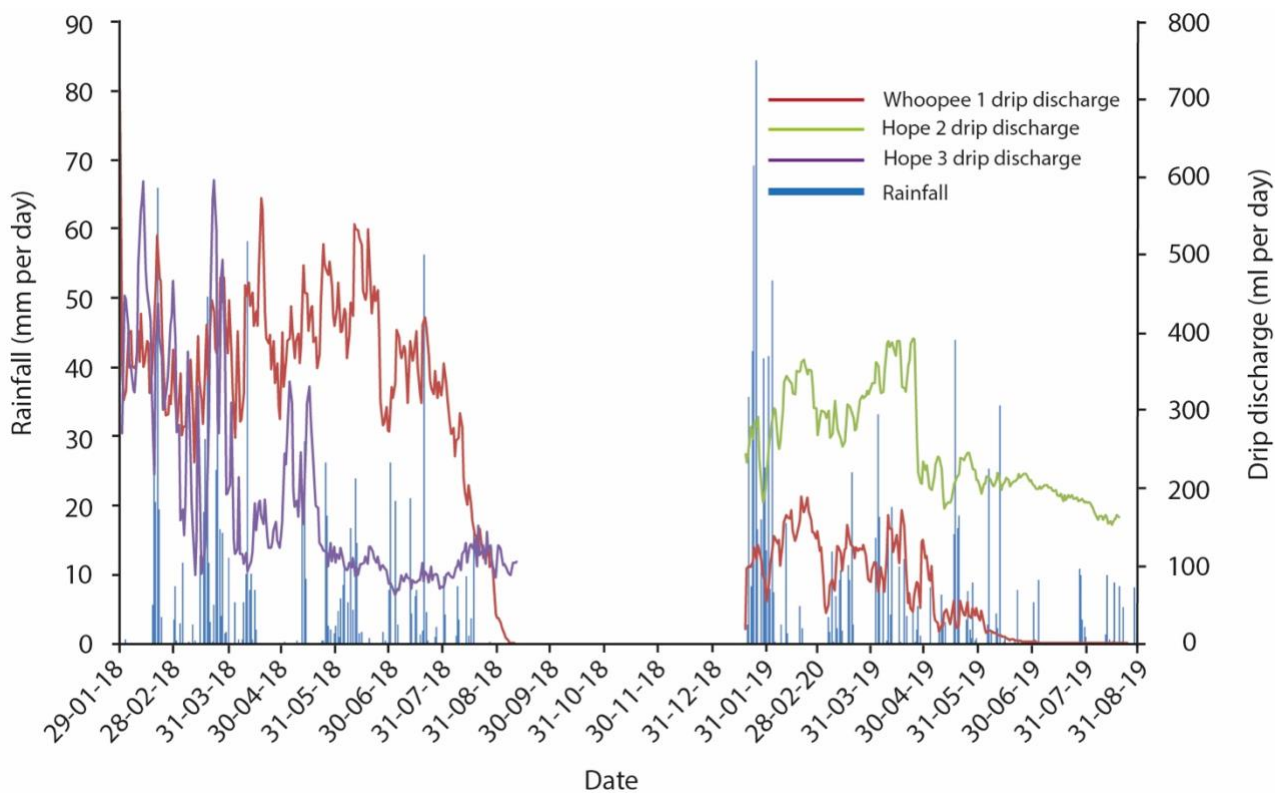


Figure S1: Rainfall and drip water discharge records at Cueva-cubío del Llanío, collected between January 2018 to September 2019.

Monthly water excess (Figure S2) (calculated following Thornthwaite et al., 1948) is recognised to be in deficit within the region between June to September (Smith et al., 2016). Within Whoopee Chamber

(Cueva-cubío del Llanío), drip rate diminishes towards flow cessation in response to the annual period of negative water excess. Flow cessation indicates drip water supply from an aquifer of limited volume within the karst. This is consistent with the limited rock overburden (5 m thickness) at this site. Drip records from Hope chamber demonstrate a more persistent flux of water into the cave, achieving minimal values during the summer months, albeit never reaching flow cessation within the duration of the logged period. Whilst all drip records are responsive to external winter rainfall events, the most dramatic excursions are apparent within High hopes chamber, suggesting a greater degree of flow path connectivity through the karst and with the surface. This degree of responsiveness diminishes during the summer months as the negative water excess prevents replenishment of the karst aquifer. Drip rate records within High Hopes Chamber are thus consistent with a well-connected karst network, fed by an aquifer of sufficient volume to enable active dripping throughout the period of negative water excess. Within Whoopee Hall, the aquifer demonstrates poorer connectivity to external rainfall events, but is of limited volume such that flow cessation occurs during the summer months of negative water excess.

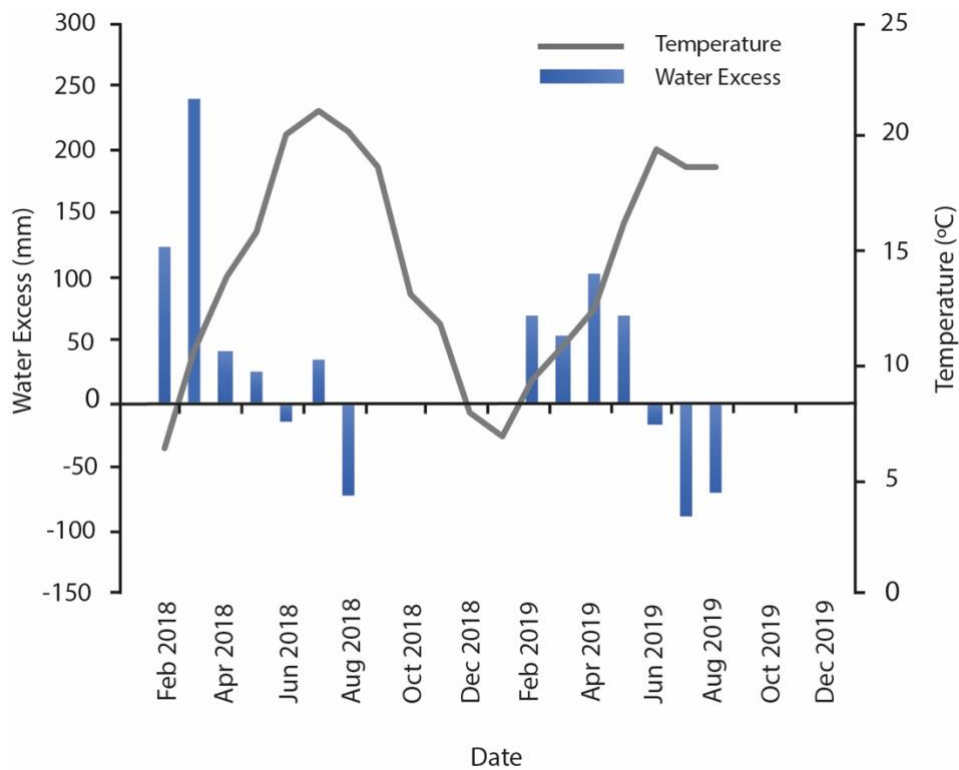


Figure S2: Monthly water excess between January 2018 to September 2019 for the Cueva-cubío del Llanío region.

References

Collister, C. and Matthey, D. 2008. Controls on water drop volume at speleothem drip sites: An experimental study. *Journal of Hydrology*, 358, 259-267.

Deeprise, L.M.C 2018. *Speleothem Climate Capture of the Neanderthal demise*. PhD, Lancaster University.

Smith, A.C., Wynn, P.M., Barker, P.A., Leng, M.J., Noble, S.R. and Stott, A. 2016. Cave monitoring and the potential for palaeoclimate reconstruction from Cueva de Asiul, Cantabria (N. Spain). *International Journal of Speleology*, 45 (1), 1-9.

THORNTHWAITE, C. W. 1948. An approach toward a rational classification of climate. *Geographical review*, 38, 55-94.